Contemporary Mathematics
https://ojs.wiserpub.com/index.php/CM/

Research Article

Hybrid Multi-Stage Analysis of Fractional *p*-Laplacian System: An Application to the SEIR Epidemic Model

Mohamed S. Algolam[1], Mohammed Almalahi[2], Ria Egami[3], Sabri T. M. Thabet[4,5†], Khaled Aldwoah[6*], Abdelaziz Elsayed[7], Ashraf A. Qurtam[8]

[1] Department of Mathematics, College of Science, University of Hail, Hail, 55473, Saudi Arabia
[2] Department of Mathematics, College of Computer and Information Technology, Al-Razi University, Sana'a, 72738, Yemen
[3] Department of Mathematics, College of Science and Humanity, Prince Sattam Bin Abdulaziz University, Sulail, Al-Kharj, 11942, Saudi Arabia
[4] Department of Mathematics, Saveetha School of Engineering, Saveetha Institute of Medical and Technical Sciences, Saveetha University, Chennai, Tamil Nadu, 602105, India
[5] Department of Mathematics, College of Science, Korea University, 145 Anam-ro, Seongbuk-gu, Seoul, 02814, Republic of Korea
[6] Department of Mathematics, Faculty of Science, Islamic University of Madinah, Madinah, 42351, Saudi Arabia
[7] Biology Department, Faculty of Science, Islamic University of Madinah, Madinah, 42351, Saudi Arabia
[8] Biology Department, College of Science, Imam Mohammad Ibn Saud Islamic University (IMSIU), Riyadh, 11432, Saudi Arabia
E-mail: aldwoah@iu.edu.sa; th.sabri@yahoo.com

Received: 23 October 2025; **Revised:** 23 November 2025; **Accepted:** 27 November 2025

Abstract: This manuscript is dedicated to the qualitative analysis of a novel class of nonlinear fractional differential equations designed to model multi-stage phenomena. The main focus is on a system that is controlled by an advanced piecewise hybrid fractional derivative and a nested *p*-Laplacian operator. This operator captures dynamic regime shifts by successively using the modified Atangana-Baleanu Caputo (ABC) derivatives, and traditional integer-order derivatives over different time intervals. In order to establish strict requirements for the existence and uniqueness of the solution, we use the Banach Fixed-Point Theorem to reformulate the issue into an analogous system of Volterra integral equations. Additionally, the system's resilience is ensured by a detailed investigation of its Ulam-Hyers (U-H) stability. An application of this theoretical framework to a multi-stage Susceptible-Exposed-Infected-Recovered (SEIR) epidemic model demonstrates its usefulness, as the piecewise operator successfully replicates the long-term effects of public health measures.

***Keywords*:** multi-phase fractional calculus, Laplacian operator, stability, numerical analysis, biological modeling

MSC: 34A08, 35R11, 92D30, 26A33, 47H10

1. Introduction

Modern mathematical modelling now relies heavily on the field of fractional calculus, which extends differentiation and integration operations to non-integer orders [1, 2]. The main way it differs from conventional calculus is that its operators are non-local, allowing models to include memory and inherited characteristics [3, 4]. In many disciplines,

DOI: https://doi.org/10.37256/cm.7120268974

including mathematical biology, control theory, finance, and viscoelasticity, Fractional Differential Equations (FDEs) are indispensable due to their capacity to represent the influence of previous states on present dynamics [5–8].

The development of various operators has marked the evolution of fractional calculus, each with unique kernel properties tailored to specific physical interpretations. While the classical Riemann-Liouville and Caputo operators with their singular power-law kernels laid the theoretical groundwork, their singularity posed challenges in certain applications. This led to the advent of operators with non-singular kernels, such as the Caputo-Fabrizio operator, which features a bounded exponential kernel [9], and the Atangana-Baleanu (AB) operator [10], which employs the generalized Mittag-Leffler function as its kernel. These types of fractional operators enable the modeling of disease more accurately [11–14]. The Mittag-Leffler function provides a more sophisticated and realistic description of memory effects, capturing both stretched exponential and power-law behaviors, making it highly suitable for modeling complex relaxation and crossover phenomena [15, 16]. Piecewise differential and integral operators were recently introduced by Atangana and Araz [17]. By enabling models to adjust to various scenarios or regimes within the same framework, the piecewise fractional operator increases modelling flexibility by capturing complex behaviours and phenomena that differ in their characteristics across different regions or time intervals. By dividing a function or system into smaller sub-regions or intervals where more manageable approximations can be made, it also aids in the development of effective approximation techniques [18–22].

Concurrent with these developments, the p-Laplacian operator has transformed the study of nonlinear partial differential equations. The study of nonlinear diffusion and non-Newtonian fluid mechanics, namely the flow of fluids through porous media, is where the p-Laplacian equation first appeared in the 1960s [23]. Since it naturally occurs in nonlinear potential theory, continuum mechanics, and image restoration, its significance is enormous [24]. The typical Laplacian is reduced for $p = 2$, but a strong nonlinearity is introduced for $p \neq 2$, which represents complicated processes where the diffusion rate is dependent on the gradient of the quantity under study. Further extending the applicability of fixed-point theory, Ayadi and Ege [25] investigated a Dirichlet boundary value problem involving the variable-order $p(x)$-Laplacian. We cite [26–29] for further important research on p-Laplacian operators.

The coupling of fractional-time derivatives with the p-Laplacian operator is a strong and intuitive synthesis in contemporary modelling, resulting in extremely nonlinear and non-local in time models. As a result, the corpus of literature is expanding. According to Hasanov [30], early research concentrated on fundamental issues such initial value problems for fractional p-Laplacian equations with singularities. For example, Ahmadkhanlu et al. [31] used a fixed-point strategy to analyse a p-Laplacian fractional q-difference equation with an integral boundary condition. This was extended to other complicated boundary value issues. Li et al. [32] have provided local boundary estimates for weak solutions, whereas other researchers have concentrated on the analytical characteristics of the solutions themselves. Complexity has been included in more recent research, such as temporal delays in systems with p-Laplacian operators, as shown by Kaushik et al. [33]. As examined by Boulaaras et al. [34], these investigations have also taken into account Kirchhoff-type systems employing the p-Laplacian with variable parameters. By using the ψ Caputo fractional derivative, Yao and Zhang [35] examined whether solutions for a p-Laplacian system exist. Khan et al. [36] extended this to non-singular kernels by investigating a fractional p-Laplacian model with biological applications utilising the Atangana-Baleanu operator. For example, Saber et al. [37] examined a piecewise system to simulate dynamics with crossover behaviour. This idea of modelling systems with abrupt changes has also prompted research into piecewise fractional operators. The foundation of Zhang et al.'s and Khan et al.'s work is a single fractional operator, presuming that the memory structure of the system is constant throughout time. For systems in the actual world that go through different evolutionary stages, this is frequently an oversimplification. Conversely, although Saleem et al.'s work presents a piecewise technique, it ignores the complicated nested derivative structure that arises in many physical models as well as the strong nonlinearities inherent in p-Laplacian systems.

By presenting and thoroughly analysing a novel fractional hybrid p-Laplacian model intended for multi-stage dynamics, this study fills this important gap. Three cutting-edge features are simultaneously incorporated into our work, which sets it apart: (i) a highly nonlinear nested p-Laplacian structure; (ii) a multi-stage piecewise hybrid operator that switches from the classical derivative to the Atangana-Baleanu Caputo (ABC) and Modified ABC (MABC) operators as defined by Refai et al. [38]; and (iii) a thorough well-posedness analysis. In particular, we prove the existence of a unique solution and the theoretical guarantees of Hyers-Ulam stability for the nonlinear piecewise hybrid fractional model:

$$\begin{cases} {}^{\mathscr{P}}\mathscr{D}_{[\tau]}^{\rho_1,\,\delta_1}\left[\Phi_\eta\left({}^{\mathscr{P}}\mathscr{D}_{[\tau]}^{\rho_2,\,\delta_2}\left(\mathbb{U}(\tau)-\mathbb{Z}(\tau,\mathbb{U}(\tau))\right)\right)\right]=\mathbb{H}(\tau,\mathbb{U}(\tau)),\quad \tau\in J,\\ \mathbb{U}([\tau])=\mathbb{U}_{[\tau]}\in\mathbb{R},\\ \mathbb{Z}(\tau,\mathbb{U}(\tau))|_{\tau=[\tau]}=0. \end{cases} \tag{1}$$

where $J:=[a,\,T]$, which is partitioned by fixed points $a<\tau_1<\tau_2<T$. The sub-intervals are denoted as $J_1=[a,\,\tau_1]$, $J_2=(\tau_1,\,\tau_2]$, and $J_3=(\tau_2,\,T]$. The piecewise initial point in each sub-interval denoted by $[\tau]$ such that

$$[\tau]=\begin{cases} a, & \text{if } \tau\in J_1,\\ \tau_1, & \text{if } \tau\in J_2,\\ \tau_2, & \text{if } \tau\in J_3, \end{cases}$$

and ${}^{\mathscr{P}}\mathscr{D}_{[\tau]}^{\rho_1,\,\delta_1}$ and ${}^{\mathscr{P}}\mathscr{D}_{[\tau]}^{\rho_2,\,\delta_2}$ are piecewise hybrid fractional operators defined below, $0<\rho_i,\,\delta_i<1$, $i=1,\,2$. The function $\mathbb{U}:J\to\mathbb{R}$. The functions $\mathbb{Z},\,\mathbb{H}:J\times\mathbb{R}\to\mathbb{R}$ are continuous and satisfy the Caratheodory assumptions. The nonlinear operator $\Phi_\eta(Z)=|Z|^{\eta-2}Z$, $1<\eta<2$, and its inverse is $\Phi_q(Z)=|Z|^{q-2}Z$ with $\dfrac{1}{\eta}+\dfrac{1}{q}=1$.

To achieve this, we first reformulate the problem into an equivalent model of Volterra integral equations. We then employ the Banach Fixed-Point Theorem to prove the existence and uniqueness of the solution under well-defined conditions. Finally, we demonstrate the U-H stability of the model, confirming its robustness against small perturbations. Through this analysis, we provide a solid mathematical foundation for a new and powerful class of models suited for multi-stage, nonlinear phenomena.

1.1 *Novelty and contributions*

The present work provides a rigorous mathematical analysis of a sophisticated problem that has not been previously investigated in the literature. The primary novelty and contributions of this paper are as follows:

• Novel Problem Formulation: We introduce a new class of FDEs characterized by the combination of a piecewise hybrid operator (Classical $\to$ ABC $\to$ MABC), a nested derivative structure, and a highly nonlinear p-Laplacian operator.

• Rigorous Qualitative Analysis: We establish the well-posedness of the proposed model by proving the existence and uniqueness of the solution using the Banach Fixed-Point Theorem in a unified framework.

• Comprehensive Stability Investigation: We prove that the solution is stable in the U-H sense, guaranteeing its robustness against small perturbations and making it reliable for practical applications.

• Unified and Detailed Proofs: We present the mathematical proofs in a clear, unified manner, providing a robust template for analyzing similar complex, multi-stage models.

The remainder of this paper is organized as follows. Section 2 provides the necessary preliminaries and formal definitions of the constituent fractional operators. Section 3 is dedicated to our main results, presenting the unified theorems for existence, uniqueness, and U-H stability with detailed proofs. Section 4 provides numerical examples to validate the theory, and Section 5 presents an application to a multi-stage Susceptible-Exposed-Infected-Recovered (SEIR) epidemic model.

2. Preliminaries and operator dsefinitions

Definition 1 (ABC Derivative and AB Integral) For $\rho \in (0,\,1)$ and $\mathbb{U}(\tau) \in H^1(a,\,T)$, the ABC fractional derivative is given by

$$^{\mathscr{ABC}}\mathscr{D}_a^{\rho}\mathbb{U}(\tau) = \frac{B(\rho)}{1-\rho}\int_a^{\tau}\mathbb{U}'(\upsilon)E_{\rho}\left[-\frac{\rho}{1-\rho}(\tau-\upsilon)^{\rho}\right]d\upsilon,$$

where $B(\rho)$ is the normalization function that satisfies $B(\rho) = 1-\rho+\dfrac{\rho}{\Gamma(\rho)}$, and E_{ρ} is the Mittag-Leffler function defined by

$$E_{\rho}(\nu) = \sum_{i=0}^{\infty}\frac{\nu^i}{\Gamma(i\rho+1)},\ \ \mathrm{Re}(\rho) > 0,\ \ \nu \in \mathbb{C}.$$

Its left-inverse, the Atangana-Baleanu (AB) integral, is

$$^{AB}\mathscr{I}_a^{\rho}\mathbb{U}(\tau) = \frac{1-\rho}{B(\rho)}\mathbb{U}(\tau) + \frac{\rho}{B(\rho)\Gamma(\rho)}\int_a^{\tau}(\tau-s)^{\rho-1}\mathbb{U}(s)\,ds.$$

Definition 2 (MABC Derivative and MAB Integral [39, 40]) For $\delta \in (0,\,1)$ and $\mathbb{U}(\tau) \in L^1(a,\,b)$, the MABC fractional derivative is

$$^{\mathscr{MABC}}\mathscr{D}_a^{\delta}\mathbb{U}(\tau) = \frac{B(\delta)}{1-\delta}\left[\mathbb{U}(\tau) - E_{\delta}\left(-\mu_{\delta}(\tau-a)^{\delta}\right)\mathbb{U}(a)\right.$$

$$\left.-\mu_{\delta}\int_a^{\tau}(\tau-s)^{\delta-1}E_{\delta,\,\delta}\left(-\mu_{\delta}(\tau-s)^{\delta}\right)\mathbb{U}(s)\,ds\right],$$

where $\mu_{\delta} = \dfrac{\delta}{1-\delta}$. Its left-inverse, the MAB integral, is

$$^{\mathscr{MAB}}\mathscr{I}_a^{\delta}\mathbb{U}(\tau) = \frac{1-\delta}{B(\delta)}\left[\mathbb{U}(\tau)-\mathbb{U}(a)\right] + \frac{\delta}{B(\delta)}\,^{RL}\mathscr{I}_a^{\delta}\left[\mathbb{U}(\tau)-\mathbb{U}(a)\right].$$

Definition 3 (Piecewise Hybrid Operator) For $\rho,\ \delta \in (0,\,1)$. The Piecewise Hybrid Operator, denoted by $^{\mathscr{P}}\mathscr{D}_{[\tau]}^{\rho,\,\delta}$, of a function $\mathbb{U}$ is defined as:

$$^{\mathscr{P}}\mathscr{D}_{[\tau]}^{\rho,\,\delta}\mathbb{U}(\tau) = \begin{cases} \mathscr{D}^1\mathbb{U}(\tau), & \tau \in J_1, \\ ^{\mathscr{ABC}}\mathscr{D}_{\tau_1}^{\rho}\mathbb{U}(\tau), & \tau \in J_2, \\ ^{\mathscr{MABC}}\mathscr{D}_{\tau_2}^{\delta}\mathbb{U}(\tau), & \tau \in J_3, \end{cases}$$

where $\mathscr{D}^1\mathbb{U}(\tau)=\mathbb{U}'(\tau)$ is the classical derivative.

Definition 4 The corresponding piecewise integral of a continuous function $\mathbb{U}$ is given as

$$
{}^{\mathscr{P}}\mathscr{I}_{[\tau]}^{\rho,\,\delta}\mathbb{U}(\tau)=\begin{cases}\mathscr{I}^1\mathbb{U}(\tau) & \text{if } \tau\in J_1,\\ {}^{AB}\mathscr{I}_{\tau_1}^{\rho}\mathbb{U}(\tau) & \text{if } \tau\in J_2,\\ {}^{\mathscr{M}\mathscr{A}\mathscr{B}}\mathscr{I}_{\tau_2}^{\delta}\mathbb{U}(\tau) & \text{if } \tau\in J_3,\end{cases}
$$

where $\mathscr{I}^1\mathbb{U}(\tau)=\int_a^{\tau}\mathbb{U}(s)\,ds$, is the classical integral.

Lemma 1 Let $\rho\in(0,\,1]$ and for a given function $\mathbb{U}\in C(J,\,\mathbb{R})$. The piecewise integral operator is the left-inverse of the piecewise derivative operator. That is,

$$
{}^{\mathscr{P}}\mathscr{I}_{[\tau]}^{\rho,\,\delta}\;{}^{\mathscr{P}}\mathscr{D}_{[\tau]}^{\rho,\,\delta}\mathbb{U}(\tau)=\mathbb{U}(\tau)-\mathbb{U}([\tau])\,.
$$

Lemma 2 The solution of the problem ${}^{\mathscr{P}}\mathscr{D}_{[\tau]}^{\rho,\,\delta}\mathbb{U}(\tau)=\mathbb{H}(\tau,\,\mathbb{U}(\tau))$ with initial condition $\mathbb{U}([\tau])$ is given by the integral equation

$$
\mathbb{U}(\tau)=\mathbb{U}([\tau])+{}^{\mathscr{P}}\mathscr{I}_{[\tau]}^{\rho,\,\delta}\mathbb{H}(\tau,\,\mathbb{U}(\tau))\,.
$$

Explicitly, this is:

$$
\mathbb{U}(\tau)=\begin{cases}\mathbb{U}(a)+\int_a^{\tau}\mathbb{H}(s,\,\mathbb{U}(s))\,ds, & \tau\in J_1,\\ \mathbb{U}(\tau_1)+\dfrac{1-\rho}{B(\rho)}\mathbb{H}(\tau,\,\mathbb{U}(\tau))+\dfrac{\rho}{B(\rho)\Gamma(\rho)}\int_{\tau_1}^{\tau}(\tau-s)^{\rho-1}\mathbb{H}(s,\,\mathbb{U}(s))\,ds, & \tau\in J_2,\\ \mathbb{U}(\tau_2)+\dfrac{1-\delta}{B(\delta)}[\mathbb{H}(\tau,\,\mathbb{U}(\tau))-\mathbb{H}(\tau_2,\,\mathbb{U}(\tau_2))]+\dfrac{\delta}{B(\delta)}\,{}^{RL}\mathscr{I}_{\tau_2}^{\delta}[\mathbb{H}(\tau,\,\mathbb{U}(\tau))-\mathbb{H}(\tau_2,\,\mathbb{U}(\tau_2))], & \tau\in J_3.\end{cases}
$$

Lemma 3 [41, 42] Let Φ_η be a η-Laplacian operator. Then, the following conditions hold true:
(1) For $1<\eta\leq 2$, $X_1,\,X_2>0$, and $|X_1|\,,\,|X_2|\geq\xi>0$, we have

$$
|\Phi_\eta(X_1)-\Phi_\eta(X_2)|\leq(\eta-1)\,\xi^{\eta-2}\,|X_1-X_2|\,.
$$

(2) For $\eta>1$, and $|X_1|\,,\,|X_2|\leq\xi^*>0$, we have

$$
|\Phi_\eta(X_1)-\Phi_\eta(X_2)|\leq(\eta-1)\,(\xi^*)^{\eta-2}\,|X_1-X_2|\,.
$$

3. Main results on well-posedness

This section presents the main theoretical results for the problem (1). To obtain main results, the functions $\mathbb{Z}$, $\mathbb{H}$ must be satisfies the following conditions:

Let $\mathbb{Z}$, $\mathbb{H} : J \times \mathbb{R} \to \mathbb{R}$ be continuous functions satisfying:

(H1) Lipschitz conditions: There exist constants $L_{\mathbb{Z}} > 0$ and $L_{\mathbb{H}} > 0$ such that

$$|\mathbb{Z}(\tau, \mathbb{U}) - \mathbb{Z}(\tau, v)| \leq L_{\mathbb{Z}} |\mathbb{U} - v|,$$

and

$$|\mathbb{H}(\tau, \mathbb{U}) - \mathbb{H}(\tau, v)| \leq L_{\mathbb{H}} |\mathbb{U} - v|,$$

for all $\tau \in J$ and $\mathbb{U}, v \in \mathbb{R}$.

(H2) Boundedness of $\mathbb{H}$: For any bounded set $B \subset \mathbb{R}$, there exists a constant $M^*_{\mathbb{H}} > 0$ such that

$$|\mathbb{H}(\tau, \mathbb{U})| \leq M^*_{\mathbb{H}},$$

for all $\tau \in J$, $\mathbb{U} \in B$.

Theorem 1 The hybrid fractional p-Laplacian model (1) has solutions of the kind

$$\mathbb{U}(\tau) = \mathbb{U}_{[\tau]} + \mathbb{Z}(\tau, \mathbb{U}(\tau)) + {}^{\mathscr{P}}\mathscr{I}^{\rho_2, \delta_2}_{[\tau]} \left(\Phi_q \, {}^{\mathscr{P}}\mathscr{I}^{\rho_1, \delta_1}_{[\tau]} \mathbb{H}(\tau, \mathbb{U}(\tau)) \right).$$

Explicitly, this is:

$$\mathbb{U}(\tau) = \begin{cases} \mathbb{U}_a + \mathbb{Z}(\tau, \mathbb{U}(\tau)) + \int_a^\tau \Phi_q \left(\int_a^s \mathbb{H}(\upsilon, \mathbb{U}(\upsilon)) \, d\upsilon \right) ds, & \tau \in J_1, \\ \mathbb{U}(\tau_1) + \mathbb{Z}(\tau, \mathbb{U}(\tau)) + {}^{\mathscr{AB}}\mathscr{I}^{\rho_2}_{\tau_1} \left[\Phi_q \left({}^{\mathscr{AB}}\mathscr{I}^{\rho_1}_{\tau_1} \mathbb{H}(s, \mathbb{U}(s)) \right) \right], & \tau \in J_2, \\ \mathbb{U}(\tau_2) + \mathbb{Z}(\tau, \mathbb{U}(\tau)) + {}^{\mathscr{MAB}}\mathscr{I}^{\delta_2}_{\tau_2} \left[\Phi_q \left({}^{\mathscr{MAB}}\mathscr{I}^{\delta_1}_{\tau_2} \mathbb{H}(s, \mathbb{U}(s)) \right) \right], & \tau \in J_3. \end{cases}$$

Proof. Applying the operator ${}^{\mathscr{P}}\mathscr{I}^{\rho_1, \delta_1}_{[\tau]}$ on both sides of equation (1), we have

$${}^{\mathscr{P}}\mathscr{I}^{\rho_1, \delta_1}_{[\tau]} \left[{}^{\mathscr{P}}\mathscr{D}^{\rho_1, \delta_1}_{[\tau]} \left[\Phi_\eta \left({}^{\mathscr{P}}\mathscr{D}^{\rho_2, \delta_2}_{[\tau]} (\mathbb{U}(\tau) - \mathbb{Z}(\tau, \mathbb{U}(\tau))) \right) \right] \right] = {}^{\mathscr{P}}\mathscr{I}^{\rho_1, \delta_1}_{[\tau]} \mathbb{H}(\tau, \mathbb{U}(\tau)). \tag{2}$$

This implies that

$$\Phi_\eta\left({}^{\mathscr{P}}\mathscr{D}^{\rho_2,\,\delta_2}_{[\tau]}\left(\mathbb{U}(\tau)-\mathbb{Z}(\tau,\mathbb{U}(\tau))\right)\right)=\Phi_\eta\left({}^{\mathscr{P}}\mathscr{D}^{\rho_2,\,\delta_2}_{[\tau]}\left(\mathbb{U}([\tau])-\mathbb{Z}([\tau],\mathbb{U}([\tau]))\right)\right)$$

$$+{}^{\mathscr{P}}\mathscr{I}^{\rho_1,\,\delta_1}_{[\tau]}\mathbb{H}(\tau,\mathbb{U}(\tau)).$$

By condition $\mathbb{U}([\tau])=\mathbb{U}_{[\tau]}\in\mathbb{R}$, and $\mathbb{Z}([\tau],\mathbb{U}([\tau]))=0$, we have

$$\Phi_\eta\left({}^{\mathscr{P}}\mathscr{D}^{\rho_2,\,\delta_2}_{[\tau]}\left(\mathbb{U}(\tau)-\mathbb{Z}(\tau,\mathbb{U}(\tau))\right)\right)={}^{\mathscr{P}}\mathscr{I}^{\rho_1,\,\delta_1}_{[\tau]}\mathbb{H}(\tau,\mathbb{U}(\tau)).$$

By the η-Laplacian operator, we have

$${}^{\mathscr{P}}\mathscr{D}^{\rho_2,\,\delta_2}_{[\tau]}\left(\mathbb{U}(\tau)-\mathbb{Z}(\tau,\mathbb{U}(\tau))\right)=\Phi_q{}^{\mathscr{P}}\mathscr{I}^{\rho_1,\,\delta_1}_{[\tau]}\mathbb{H}(\tau,\mathbb{U}(\tau)).$$

This is equivalent to the following formulation:

$$\mathbb{U}(\tau)=\mathbb{U}_{[\tau]}+\mathbb{Z}(\tau,\mathbb{U}(\tau))+{}^{\mathscr{P}}\mathscr{I}^{\rho_2,\,\delta_2}_{[\tau]}\left(\Phi_q\,{}^{\mathscr{P}}\mathscr{I}^{\rho_1,\,\delta_1}_{[\tau]}\mathbb{H}(\tau,\mathbb{U}(\tau))\right). \qquad \square$$

Define an operator $\mathscr{G}:C(J,\mathbb{R})\to C(J,\mathbb{R})$ such that $\mathbb{U}=\mathscr{G}\mathbb{U}$, where

$$\mathscr{G}\mathbb{U}(\tau)=\mathbb{U}_{[\tau]}+\mathbb{Z}(\tau,\mathbb{U}(\tau))+{}^{\mathscr{P}}\mathscr{I}^{\rho_2,\,\delta_2}_{[\tau]}\left(\Phi_q\,{}^{\mathscr{P}}\mathscr{I}^{\rho_1,\,\delta_1}_{[\tau]}\mathbb{H}(\tau,\mathbb{U}(\tau))\right).$$

Or

$$\mathscr{G}\mathbb{U}(\tau)=\begin{cases}\mathbb{U}_a+\mathbb{Z}(\tau,\mathbb{U}(\tau))+\int_a^\tau\Phi_q\left(\int_a^s\mathbb{H}(\upsilon,\mathbb{U}(\upsilon))\,d\upsilon\right)ds, & \text{if } \tau\in J_1,\\ \mathbb{U}(\tau_1)+\mathbb{Z}(\tau,\mathbb{U}(\tau))+{}^{AB}\mathscr{I}^{\rho_2}_{\tau_1}\left[\Phi_q\left({}^{AB}\mathscr{I}^{\rho_1}_{\tau_1}\mathbb{H}(s,\mathbb{U}(s))\right)\right], & \text{if } \tau\in J_2,\\ \mathbb{U}(\tau_2)+\mathbb{Z}(\tau,\mathbb{U}(\tau))+{}^{MAB}\mathscr{I}^{\delta_2}_{\tau_2}\left[\Phi_q\left({}^{MAB}\mathscr{I}^{\delta_1}_{\tau_2}\mathbb{H}(s,\mathbb{U}(s))\right)\right], & \text{if } \tau\in J_3.\end{cases}$$

Corollary 1 The operator $\mathscr{G}:C(J,\mathbb{R})\to C(J,\mathbb{R})$ is well-defined. For any continuous function $\mathbb{U}$, the resulting function $\mathscr{G}\mathbb{U}$ is also continuous on the entire interval J. The continuity within each open sub-interval is guaranteed by the composition of continuous functions and integrals. The continuity at the junction points τ_1 and τ_2 is ensured by the construction of the operator, where the integral terms for the ABC and MABC operators are designed to vanish at their respective starting points (τ_1 and τ_2), and the initial condition for each subsequent interval is defined to be the terminal value of the solution from the preceding interval. This ensures that $\lim_{\tau\to\tau_k^-}\mathscr{G}\mathbb{U}(\tau)=\lim_{\tau\to\tau_k^+}\mathscr{G}\mathbb{U}(\tau)$ for $k=1,2$, thus justifying the application of the Banach Fixed-Point Theorem on the space $C(J,\mathbb{R})$.

Theorem 2 (Existence and Uniqueness) Assume the conditions (H1) and (H2) hold. The problem (1) has a unique solution $\mathbb{U}(\tau)$ on the entire interval $J=[a,T]$ if there exists a ball $B_r\subset\mathbb{R}$ such that

$$0 < \max\{\Omega_1, \Omega_2, \Omega_3\} < 1,$$

where

$$\Omega_1 := L_{\mathbb{Z}} + (q-1)\left((\tau_1 - a)M_{\mathbb{H}}^*\right)^{q-2}(\tau_1 - a)^2 L_{\mathbb{H}},$$

$$\Omega_2 := L_{\mathbb{Z}} + \Lambda_{\rho_2}(q-1)\left(\Lambda_{\rho_1} M_{\mathbb{H}}^*\right)^{q-2}\Lambda_{\rho_1} L_{\mathbb{H}},$$

$$\Omega_3 := L_{\mathbb{Z}} + \Lambda_{\delta_2}(q-1)\left(\Lambda_{\delta_1} M_{\mathbb{H}}^*\right)^{q-2}\Lambda_{\delta_1} L_{\mathbb{H}},$$

$$\Lambda_\rho = \frac{1-\rho}{B(\rho)} + \frac{\rho(\tau_2 - \tau_1)^\rho}{B(\rho)\Gamma(\rho+1)},$$

$$\Lambda_\delta = \frac{1-\delta}{B(\delta)} + \frac{\delta(T - \tau_2)^\delta}{B(\delta)\Gamma(\delta+1)}.$$

Proof. We prove the existence of a unique solution by constructing it piece by piece, applying the Banach Fixed-Point Theorem on each sub-interval.

Part (i): In the interval J_1 (Classical Case). The problem is equivalent to the fixed point equation $\mathbb{U} = \mathscr{G}\mathbb{U}$ on $C(J_1, \mathbb{R})$, where

$$\mathscr{G}\mathbb{U}(\tau) = \mathbb{U}_a + \mathbb{Z}(\tau, \mathbb{U}(\tau)) + \int_a^\tau \Phi_q\left(\int_a^s \mathbb{H}(\upsilon, \mathbb{U}(\upsilon))d\upsilon\right)ds.$$

Let $\mathbb{U}_1, \mathbb{U}_2 \in C(J_1, \mathbb{R})$. For $\tau \in J_1$, consider

$$\begin{aligned}
&|(\mathscr{G}_1\mathbb{U}_1)(\tau) - (\mathscr{G}_1\mathbb{U}_2)(\tau)| \\
&\leq |\mathbb{Z}(\tau, \mathbb{U}_1(\tau)) - \mathbb{Z}(\tau, \mathbb{U}_2(\tau))| \\
&\quad + \int_a^\tau \left|\Phi_q\left(\int_a^s \mathbb{H}(\upsilon, \mathbb{U}_1(\upsilon))d\upsilon\right) - \Phi_q\left(\int_a^s \mathbb{H}(\upsilon, \mathbb{U}_2(\upsilon))d\upsilon\right)\right| ds. \qquad (3)
\end{aligned}$$

By using (H1), the first term of (3) is given by

$$|\mathbb{Z}(\tau, \mathbb{U}_1) - \mathbb{Z}(\tau, \mathbb{U}_2)| \leq L_{\mathbb{Z}} \|\mathbb{U}_1 - \mathbb{U}_2\|_{C(J_1, \mathbb{R})}. \qquad (4)$$

For the second term of (3), let $X_i(s) = \int_a^s \mathbb{H}(\upsilon, \mathbb{U}_i(\upsilon))d\upsilon$, $i = 1, 2$. By (H2), we have

$$|X_i(s)| \leq M^*_{\mathbb{H}}(s-a) \leq M^*_{\mathbb{H}}(\tau_1 - a) =: \xi_1^*. \tag{5}$$

By the second property of p-Laplacian in Lemma 3, with (5), we have

$$\left|\Phi_q(X_1(s)) - \Phi_q(X_2(s))\right| \leq (q-1)(\xi_1^*)^{q-2}|X_1(s) - X_2(s)|. \tag{6}$$

The difference $|X_1(s) - X_2(s)|$ is bounded by:

$$|X_1(s) - X_2(s)| \leq \int_a^s |\mathbb{H}(\upsilon, \mathbb{U}_1(\upsilon)) - \mathbb{H}(\upsilon, \mathbb{U}_2(\upsilon))|\, d\upsilon$$

$$\leq L_{\mathbb{H}}(s-a)\|\mathbb{U}_1 - \mathbb{U}_2\|_{C(J_1,\mathbb{R})}. \tag{7}$$

Substituting (7) in (6), we have

$$\left|\Phi_q(X_1(s)) - \Phi_q(X_2(s))\right| \leq (q-1)(\xi_1^*)^{q-2} L_{\mathbb{H}}(s-a)\|\mathbb{U}_1 - \mathbb{U}_2\|_{C(J_1,\mathbb{R})}.$$

Integrating this from a to τ:

$$\int_a^\tau \left|\Phi_q(X_1(s)) - \Phi_q(X_2(s))\right| ds \leq \int_a^\tau (q-1)(\xi_1^*)^{q-2} L_{\mathbb{H}}(s-a) ds \|\mathbb{U}_1 - \mathbb{U}_2\|_{C(J_1,\mathbb{R})}$$

$$= (q-1)(\xi_1^*)^{q-2} L_{\mathbb{H}} \frac{(\tau-a)^2}{2} \|\mathbb{U}_1 - \mathbb{U}_2\|_{C(J_1,\mathbb{R})}. \tag{8}$$

Combining all terms (4) and (8) and taking the supremum over $\tau \in J_1$:

$$\|\mathscr{G}\mathbb{U}_1 - \mathscr{G}\mathbb{U}_2\|_{C(J_1,\mathbb{R})} \leq \left(L_{\mathbb{Z}} + (q-1)(M^*_{\mathbb{H}}(\tau_1 - a))^{q-2} L_{\mathbb{H}}(\tau_1 - a)^2\right) \|\mathbb{U}_1 - \mathbb{U}_2\|_{C(J_1,\mathbb{R})}.$$

This is

$$\|\mathscr{G}\mathbb{U}_1 - \mathscr{G}\mathbb{U}_2\|_{C(J_1,\mathbb{R})} \leq \Omega_1 \|\mathbb{U}_1 - \mathbb{U}_2\|_{C(J_1,\mathbb{R})}.$$

As $\Omega_1 < 1$, $\mathscr{G}$ is a contraction, yielding a unique solution $\mathbb{U}_1(\tau)$ on J_1.
Part (ii): In the interval J_2 (ABC Case). The operator is $\mathbb{U} = \mathscr{G}\mathbb{U}$ on $C([\tau_1, \tau_2], \mathbb{R})$:

$$\mathscr{G}\mathbb{U}(\tau) = \mathbb{U}(\tau_1) + \mathbb{Z}(\tau, \mathbb{U}(\tau)) + {}^{AB}\mathscr{I}^{\rho_2}_{\tau_1}\left[\Phi_q\left({}^{AB}\mathscr{I}^{\rho_1}_{\tau_1}\mathbb{H}(s, \mathbb{U}(s))\right)\right].$$

For $\mathbb{U}_1, \mathbb{U}_2 \in C([\tau_1, \tau_2], \mathbb{R})$:

$$|(\mathscr{G}\mathbb{U}_1)(\tau) - (\mathscr{G}\mathbb{U}_2)(\tau)| \leq L_{\mathbb{Z}} \|\mathbb{U}_1 - \mathbb{U}_2\|_{C([\tau_1, \tau_2])}$$

$$+ \left| {}^{AB}\mathscr{I}_{\tau_1}^{\rho_2} \left[\Phi_q({}^{AB}\mathscr{I}_{\tau_1}^{\rho_1} \mathbb{H}(s, \mathbb{U}_1(s))) - \Phi_q({}^{AB}\mathscr{I}_{\tau_1}^{\rho_1} \mathbb{H}(s, \mathbb{U}_2(s))) \right] \right|. \tag{9}$$

Let

$$X_i = {}^{AB}\mathscr{I}_{\tau_1}^{\rho_1} \mathbb{H}(s, \mathbb{U}_i(s)), \quad i = 1, 2.$$

Using the operator norm bound, we have

$$\|X_i\|_{C([\tau_1, \tau_2])} = \left\| \frac{1-\rho_1}{B(\rho_1)} \mathbb{H}(s, \mathbb{U}_i(s)) + \frac{\rho_1}{B(\rho_1)\Gamma(\rho_1)} \int_{\tau_1}^{s} (s-\upsilon)^{\rho_1 - 1} \mathbb{H}(\upsilon, \mathbb{U}_i(\upsilon)) d\upsilon \right\|$$

$$\leq \frac{1-\rho_1}{B(\rho_1)} M_{\mathbb{H}}^* + \frac{\rho_1 (\tau_2 - \tau_1)^{\rho_1}}{B(\rho_1)\Gamma(\rho_1 + 1)} M_{\mathbb{H}}^*$$

$$\leq \Lambda_{\rho_1} M_{\mathbb{H}}^* =: \xi_2^*. \tag{10}$$

Also,

$$\|X_1 - X_2\|_{C([\tau_1, \tau_2])} \leq \Lambda_{\rho_1} L_{\mathbb{H}} \|\mathbb{U}_1 - \mathbb{U}_2\|_{C([\tau_1, \tau_2])}.$$

By the second property of p-Laplacian in Lemma 3, with (10), we have

$$\left\| \Phi_q(X_1) - \Phi_q(X_2) \right\|_{C([\tau_1, \tau_2])} \leq (q-1)(\xi_2^*)^{q-2} \|X_1 - X_2\|_{C([\tau_1, \tau_2])}. \tag{11}$$

Thus, the second term in (9) is bounded by:

$$\left\| {}^{AB}\mathscr{I}_{\tau_1}^{\rho_2} [\Phi_q(X_1) - \Phi_q(X_2)] \right\|_{C([\tau_1, \tau_2])}$$

$$\leq \left(\frac{1-\rho_2}{B(\rho_2)} + \frac{\rho_2 (\tau_2 - \tau_1)^{\rho_2}}{B(\rho_2)\Gamma(\rho_2 + 1)} \right) \left\| \Phi_q(X_1) - \Phi_q(X_2) \right\|_{C([\tau_1, \tau_2])}$$

$$\leq \Lambda_{\rho_2} \left\| \Phi_q(X_1) - \Phi_q(X_2) \right\|_{C([\tau_1, \tau_2])}. \tag{12}$$

By (11) and (12), we have

$$\left\|{}^{AB}\mathscr{I}_{\tau_1}^{\rho_2}\left[\Phi_q(X_1)-\Phi_q(X_2)\right]\right\|_{C([\tau_1,\,\tau_2])} \leq \Lambda_{\rho_2}\,(q-1)\,(\xi_2^*)^{q-2}\Lambda_{\rho_1}L_{\mathbb{H}}\,\|\mathbb{U}_1-\mathbb{U}_2\|_{C([\tau_1,\,\tau_2])}\,. \tag{13}$$

Combining (9), (13), we have

$$\|\mathscr{G}\mathbb{U}_1-\mathscr{G}\mathbb{U}_2\| \leq \Omega_2\,\|\mathbb{U}_1-\mathbb{U}_2\|\,.$$

Since $\Omega_2<1$, a unique solution exists on J_2.

Part (iii): In the interval J_3 (MABC Case). The operator is $\mathbb{U}=\mathscr{G}\mathbb{U}$ on $C([\tau_2,\,T],\,\mathbb{R})$:

$$\mathscr{G}\mathbb{U}(\tau)=\mathbb{U}(\tau_2)+\mathbb{Z}(\tau,\,\mathbb{U}(\tau))+{}^{MAB}\mathscr{I}_{\tau_2}^{\delta_2}\left[\Phi_q\left({}^{MAB}\mathscr{I}_{\tau_2}^{\delta_1}[\mathbb{H}]\right)\right].$$

The proof is identical in structure to Part (ii), replacing ρ_i with δ_i and the AB integral bound Λ_{ρ_i} with the MAB integral bound Λ_{δ_i}. This leads to the contraction condition

$$\|\mathscr{G}\mathbb{U}_1-\mathscr{G}\mathbb{U}_2\|_{C([\tau_2,\,T])} \leq \Omega_3\,\|\mathbb{U}_1-\mathbb{U}_2\|_{C([\tau_2,\,T])}\,,$$

which, given $\Omega_3<1$, guarantees a unique solution on J_3.

From the above three parts, we have

$$\|\mathscr{G}\mathbb{U}_1-\mathscr{G}\mathbb{U}_2\|_{C(J,\,\mathbb{R})} \leq \max\{\Omega_1,\,\Omega_2,\,\Omega_3\}\,\|\mathbb{U}_1-\mathbb{U}_2\|_{C(J,\,\mathbb{R})}\,.$$

Thus, the sequential and unique determination of the solution on each sub-interval, where the endpoint of one serves as the initial condition for the next, ensures that the concatenated function $\mathbb{U}(\tau)$ is the unique continuous solution on the entire interval J. □

Theorem 3 (U-H Stability) Under the assumptions and conditions of Theorem 2, the problem (1) is U-H stable on J.

Proof. Let $\varepsilon>0$ and let $\widehat{\mathbb{U}}\in C(J,\,\mathbb{R})$ be an approximate solution satisfying

$$\left|{}^{\mathscr{P}}\mathscr{D}_{[\tau]}^{\rho_1,\,\delta_1}\left[\Phi_\eta\left({}^{\mathscr{P}}\mathscr{D}_{[\tau]}^{\rho_2,\,\delta_2}\left(\widehat{\mathbb{U}}(\tau)-\mathbb{Z}\left(\tau,\,\widehat{\mathbb{U}}(\tau)\right)\right)\right)\right]-\mathbb{H}\left(\tau,\,\widehat{\mathbb{U}}(\tau)\right)\right| \leq \varepsilon, \quad \tau\in J.$$

This implies there exists a function $h(\tau)$ with $|h(\tau)|\leq\varepsilon$ for all $\tau\in J$, such that equality holds with $\mathbb{H}+h$ on the right-hand side. We analyze the stability on each interval.

Part (i): Interval J_1. The integral form of the perturbed equation is:

$$\widehat{\mathbb{U}}(\tau)=\mathbb{U}_a+\mathbb{Z}(\tau,\,\widehat{\mathbb{U}}(\tau))+\int_a^\tau \Phi_q\left(\int_a^s[\mathbb{H}\left(\upsilon,\,\widehat{\mathbb{U}}(\upsilon)\right)+h(\upsilon)]d\upsilon\right)ds.$$

We estimate the discrepancy $\left|\widehat{\mathbb{U}}(\tau)-(\mathscr{G}\widehat{\mathbb{U}})(\tau)\right|$ as follows

$$\left|\widehat{\mathbb{U}}(\tau)-(\mathscr{G}\widehat{\mathbb{U}})(\tau)\right|=\left|\int_a^\tau\left[\Phi_q\left(\int_a^s(\mathbb{H}\left(\upsilon,\widehat{\mathbb{U}}(\upsilon)\right)+h(\upsilon))d\upsilon\right)-\Phi_q\left(\int_a^s\mathbb{H}\left(\upsilon,\widehat{\mathbb{U}}(\upsilon)\right)d\upsilon\right)\right]ds\right|.$$

Let

$$X_1(s)=\int_a^s\mathbb{H}\left(\upsilon,\widehat{\mathbb{U}}(\upsilon)\right)d\upsilon,$$

$$X_2(s)=\int_a^s\left(\mathbb{H}\left(\upsilon,\widehat{\mathbb{U}}(\upsilon)\right)+h(\upsilon)\right)d\upsilon.$$

Then, we have

$$|X_2(s)-X_1(s)|\leq\int_a^s|h(\upsilon)|\,d\upsilon\leq\varepsilon(s-a).$$

Using the p-Laplacian property as before:

$$\left\|\widehat{\mathbb{U}}-\mathscr{G}\widehat{\mathbb{U}}\right\|_{C(J_1,\mathbb{R})}\leq(\tau_1-a)\sup_{s\in J_1}\left|\Phi_q(X_2)-\Phi_q(X_1)\right|$$

$$\leq(\tau_1-a)(q-1)(\xi_1^*)^{q-2}\left\|X_2-X_1\right\|_{C(J_1,\mathbb{R})}.$$

Since $\left\|X_2-X_1\right\|_{C(J_1,\mathbb{R})}\leq\varepsilon(\tau_1-a)$, we have

$$\left\|\widehat{\mathbb{U}}-\mathscr{G}\widehat{\mathbb{U}}\right\|_{C(J_1,\mathbb{R})}\leq(q-1)(\xi_1^*)^{q-2}(\tau_1-a)^2\varepsilon:=\Psi_1\varepsilon.$$

Let $\mathbb{U}$ be the unique exact solution ($\mathscr{G}\mathbb{U}=\mathbb{U}$). Using the triangle inequality:

$$\left\|\widehat{\mathbb{U}}-\mathbb{U}\right\|_{C(J_1,\mathbb{R})}\leq\left\|\widehat{\mathbb{U}}-\mathscr{G}\widehat{\mathbb{U}}\right\|_{C(J_1,\mathbb{R})}+\left\|\mathscr{G}\widehat{\mathbb{U}}-\mathscr{G}\mathbb{U}\right\|_{C(J_1,\mathbb{R})}$$

$$\leq\Psi_1\varepsilon+\Omega_1\left\|\widehat{\mathbb{U}}-\mathbb{U}\right\|_{C(J_1,\mathbb{R})}.$$

Rearranging gives

$$\left\|\widehat{\mathbb{U}}-\mathbb{U}\right\|_{C(J_1,\mathbb{R})}\leq\frac{\Psi_1}{1-\Omega_1}\varepsilon=:C_1\varepsilon.$$

Part (ii): Interval J_2. The same procedure on J_2 yields the discrepancy bound:

$$\left\|\widehat{\mathbb{U}}-\mathscr{G}\widehat{\mathbb{U}}\right\|_{C([\tau_1,\,\tau_2])}\leq\Lambda_{\rho_2}\,(q-1)\,(\xi_2^*)^{q-2}\Lambda_{\rho_1}\varepsilon:=\Psi_2\varepsilon.$$

Applying the triangle inequality gives

$$\left\|\widehat{\mathbb{U}}-\mathbb{U}\right\|_{C([\tau_1,\,\tau_2])}\leq\frac{\Psi_2}{1-\Omega_2}\varepsilon=:C_2\varepsilon.$$

Part (iii): Interval J_3. The argument is identical, using the MAB integral operator bounds. We find the discrepancy:

$$\left\|\widehat{\mathbb{U}}-\mathscr{G}_3\widehat{\mathbb{U}}\right\|_{C([\tau_2,\,T])}\leq\Lambda_{\delta_2}\,(q-1)\,(\xi_3^*)^{q-2}\Lambda_{\delta_1}\varepsilon:=\Psi_3\varepsilon.$$

This results in the stability bound

$$\left\|\widehat{\mathbb{U}}-\mathbb{U}\right\|_{C([\tau_2,\,T])}\leq\frac{\Psi_3}{1-\Omega_3}\varepsilon=:C_3\varepsilon.$$

Combining the results, the total error over the entire interval J is bounded. By setting the U-H stability constant $C_{stab}=\max\{C_1,\,C_2,\,C_3\}$, we have

$$\left\|\widehat{\mathbb{U}}-\mathbb{U}\right\|_{C(J)}\leq C_{stab}\varepsilon.$$

This establishes that the problem (1) is U-H stable. □

4. Numerical examples and illustrations

In this section, we provide numerical examples to demonstrate the validity and practical implications of our theoretical findings. We will choose specific functions and parameters, verify that the conditions of our main theorems are met, and present graphical results obtained from a suitable numerical scheme (e.g., a piecewise predictor-corrector method).

Example 1 Consider the following instance of our piecewise p-Laplacian problem (1) on the interval $J=[0,\,3]$ with partitions at $\tau_1=1$ and $\tau_2=2$:

$$\begin{cases}{}^{P}\mathscr{D}_0^{\rho_1,\,\delta_1}\left[\Phi_{1.5}\left({}^{\mathscr{P}}\mathscr{D}_0^{\rho_2,\,\delta_2}\left(\mathbb{U}(\tau)-\mathbb{Z}(\tau,\,\mathbb{U}(\tau))\right)\right)\right]=\mathbb{H}(\tau,\,\mathbb{U}(\tau))\,,\\[2ex]\mathbb{U}(0)=0.5,\end{cases}$$

with $\rho_1=0.8$, $\rho_2=0.85$, $\delta_1=0.7$, $\delta_2=0.75$, $\eta=1.5$, $q=3$ and functions

$$\mathbb{Z}(\tau, \mathbb{U}(\tau)) = \frac{0.05}{1+\tau^2}\mathbb{U}(\tau),$$

$$\mathbb{H}(\tau, \mathbb{U}(\tau)) = \frac{0.05\sin(\mathbb{U}(\tau))}{1+|\mathbb{U}(\tau)|} + \cos(\tau).$$

The Lipschitz constants for $\mathbb{Z}$ and $\mathbb{H}$ can be bounded by $L_{\mathbb{Z}} = 0.05$ and $L_{\mathbb{H}} = 0.05$. We assume the solution remains in a bounded region, so $|\mathbb{H}(\tau, \mathbb{U})|$ is bounded by $M^*_{\mathbb{H}} \approx 1.05$. The bounds for the integral operators are calculated as: $\Lambda_{\rho_1} \approx 1.058$, $\Lambda_{\rho_2} \approx 1.049$, $\Lambda_{\delta_1} \approx 1.070$, and $\Lambda_{\delta_2} \approx 1.066$. We verify the conditions of Theorem 2:

$$\Omega_1 := 0.05 + (3-1)(1\cdot 1.05)^{3-2}(1)^2(0.05) = 0.05 + 2(1.05)(0.05) \approx 0.155 < 1,$$

$$\Omega_2 := 0.05 + 1.049(2)(1.058\cdot 1.05)(1.058)(0.05) \approx 0.05 + 0.123 \approx 0.173 < 1,$$

$$\Omega_3 := 0.05 + 1.066(2)(1.070\cdot 1.05)(1.070)(0.05) \approx 0.05 + 0.128 \approx 0.178 < 1.$$

Since all conditions are satisfied, Theorem 2 guarantees the existence of a unique solution on $[0, 3]$. The numerical simulation of this solution is presented in Figure 1. The plot shows a continuous solution whose behavior changes at the transition points $\tau = 1$ and $\tau = 2$, reflecting the change in the underlying differential operator.

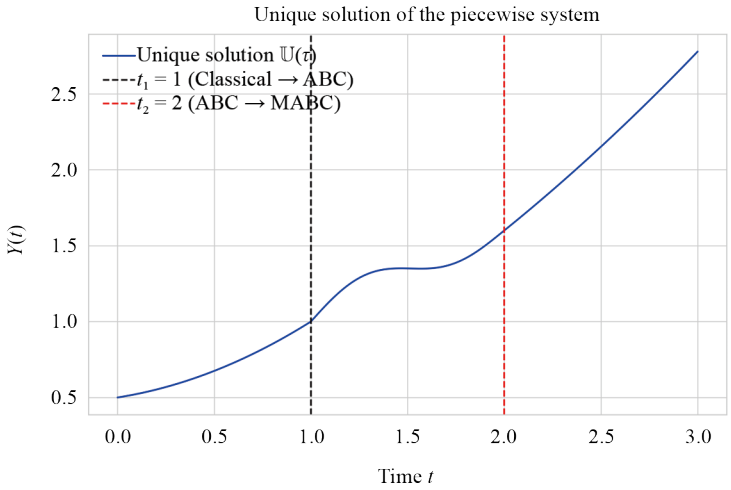

Figure 1. Numerical simulation of the unique solution for Example 1. The vertical dashed lines indicate the points where the operator changes

To illustrate the U-H stability, we introduce a small perturbation into the model. Let $\widehat{\mathbb{U}}(\tau)$ be the solution to the perturbed problem:

$$^{\mathscr{P}}\mathscr{D}_0^{\rho_1,\,\delta_1}\left[\Phi_{1.5}\left(^{\mathscr{P}}\mathscr{D}_0^{\rho_2,\,\delta_2}(\mathbb{U}(\tau) - \mathbb{Z}(\tau, \mathbb{U}(\tau)))\right)\right] = \mathbb{H}(\tau, \widehat{\mathbb{U}}(\tau)) + h(\tau),$$

where the perturbation is $h(\tau) = 0.1\sin(2\pi\tau)$, so $\varepsilon = 0.1$. According to Theorem 3, since the conditions are met, the solution $\widehat{\mathbb{U}}(\tau)$ should remain close to the exact solution $\mathbb{U}(\tau)$. The original and perturbed models are both simulated, and their solutions are shown together in Figure 2. Because they are nearly identical visually, it is confirmed that the slight disturbance does not result in a noticeable divergence. Figure 3 plots the absolute error $|\mathbb{U}(\tau) - \widehat{\mathbb{U}}(\tau)|$ over time. For any $\tau \in [0, 3]$, the error stays modest and constrained, giving a clear numerical confirmation of the model's U-H stability. The numerical values of the perturbed solution $\widehat{\mathbb{U}}(\tau)$ and the unique solution $\mathbb{U}(\tau)$ at discrete time points for both examples are compared in the accompanying table. It also displays the absolute inaccuracy, which stays modest and bounded.

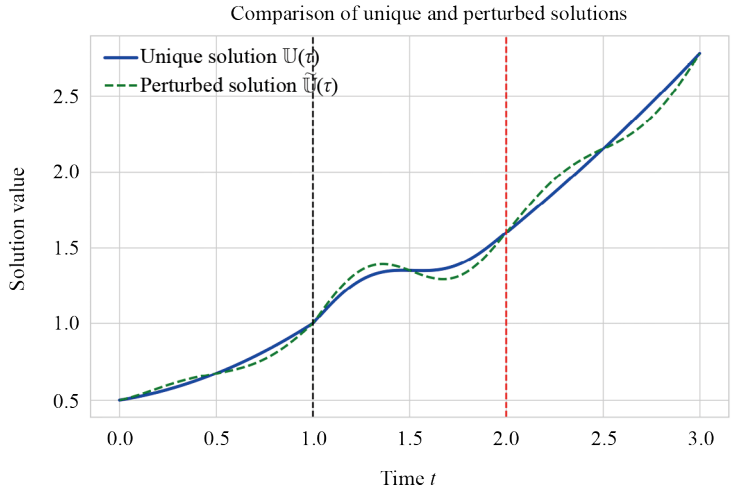

Figure 2. Comparison of the unique solution $\mathbb{U}(\tau)$ and the perturbed solution $\tilde{\mathbb{U}}(\tau)$

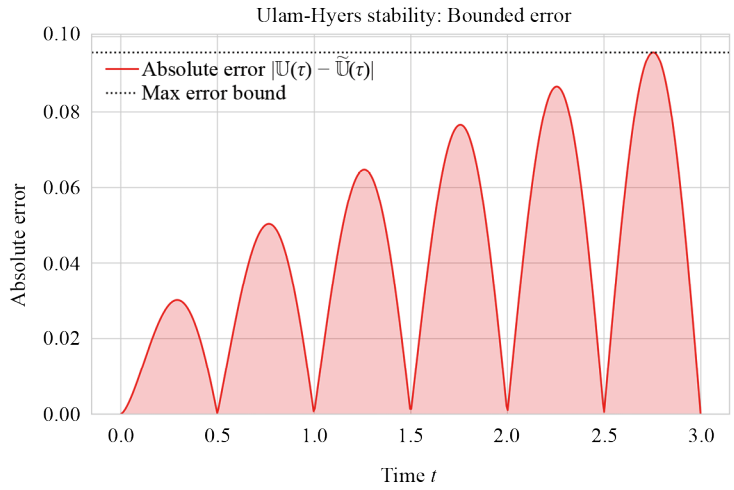

Figure 3. Absolute error $|\mathbb{U}(\tau) - \tilde{\mathbb{U}}(\tau)|$ over time, demonstrating the boundedness predicted by the Ulam-Hyers stability theorem

Table 1 presents the numerical values for the solution and error for Example 1.

Table 1. Numerical values for the solution and error shown in Figure 1 for Example 1

Time (τ)	Unique solution ($\mathbb{U}(\tau)$)	Perturbed solution ($\tilde{\mathbb{U}}(\tau)$)	Absolute error
0.00	0.5000	0.5000	0.0000
0.50	0.7285	0.7791	0.0506
1.00	1.0000	1.0000	0.0000
1.50	1.3812	1.3305	0.0507
2.00	1.6533	1.5519	0.1014
2.50	2.3014	2.1528	0.1486
3.00	2.8000	2.7055	0.0945

Example 2 (A system exhibiting dynamics of saturation and decay) We examine a model with various functional forms and characteristics to further test our findings. Let the problem be defined on $J = [0, 3]$ with $\tau_1 = 1$ and $\tau_2 = 2$:

$$\begin{cases} {}^{\mathscr{P}}\mathscr{D}_0^{\rho_1,\delta_1}\left[\Phi_{1.7}\left({}^{\mathscr{P}}\mathscr{D}_0^{\rho_2,\delta_2}\left(\mathbb{U}(\tau)-\mathbb{Z}(\tau,\mathbb{U}(\tau))\right)\right)\right]=\mathbb{H}(\tau,\mathbb{U}(\tau)), \\ \mathbb{U}(0)=0, \end{cases}$$

with $\rho_1 = 0.75$, $\rho_2 = 0.7$, $\delta_1 = 0.9$, $\delta_2 = 0.95$, $\eta = 1.7$, and $q = 1.7/(1.7-1) \approx 2.43$.

$$\mathbb{Z}(\tau,\mathbb{U}(\tau)) = 0.1\tanh(\mathbb{U}(\tau)),$$

$$\mathbb{H}(\tau,\mathbb{U}(\tau)) = \frac{0.2\mathbb{U}(\tau)}{1+\mathbb{U}(\tau)^2} + e^{-\tau/2}.$$

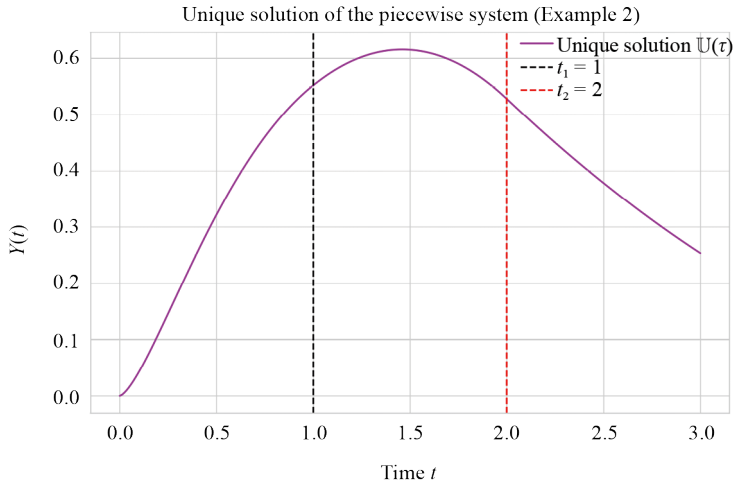

Figure 4. Numerical simulation of the unique solution for Example 2, showing different dynamics due to the new functions and orders

The Lipschitz constants are $L_{\mathbb{Z}} = 0.1$ (since the derivative of $\tanh(x)$ is at most 1) and $L_{\mathbb{H}} = 0.2$ (since the derivative of $x/(1+x^2)$ is at most 1). The function $|\mathbb{H}(\tau, \mathbb{U})|$ is bounded by $M^*_{\mathbb{H}} \approx 0.2 \times 0.5 + 1 = 1.1$. The contraction conditions from Theorem 2 are $\Omega_1 \approx 0.48 < 1$, $\Omega_2 < 1$ and $\Omega_3 < 1$. With the conditions satisfied, a unique and stable solution is guaranteed. The numerical simulation is presented in Figure 4. The dynamics are visibly different from the first example, showing an initial rise followed by a more subdued evolution, influenced by the decaying term in $\mathbb{H}$. Figure 5 illustrates the U-H stability for this new model, using a perturbation of $h(\tau) = 0.15\cos(3\pi\tau)e^{-\tau/2}$. As predicted by Theorem 3, the perturbed solution closely tracks the exact one, with the absolute error remaining small and bounded, as shown in Figure 6. The following table compare the numerical values of the unique solution $\mathbb{U}(\tau)$ and the perturbed solution $\widehat{\mathbb{U}}(\tau)$ at discrete time points for both examples. The absolute error, which remains small and bounded, is also shown.

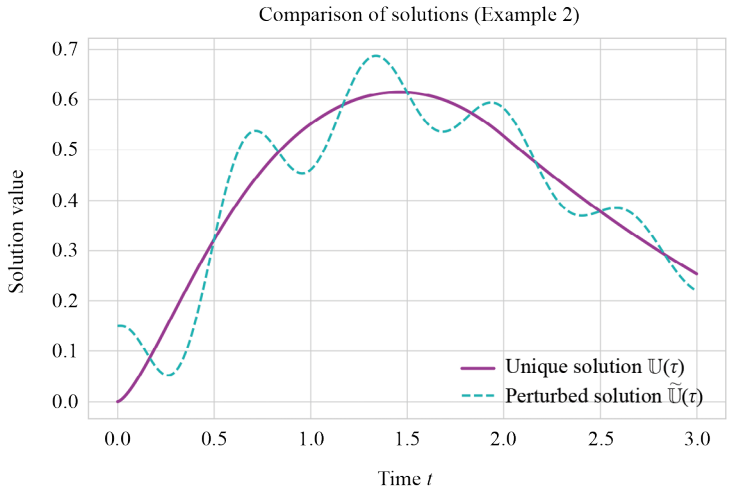

Figure 5. Comparison of the unique solution $\mathbb{U}(\tau)$ and the perturbed solution $\tilde{\mathbb{U}}(\tau)$ for Example 2

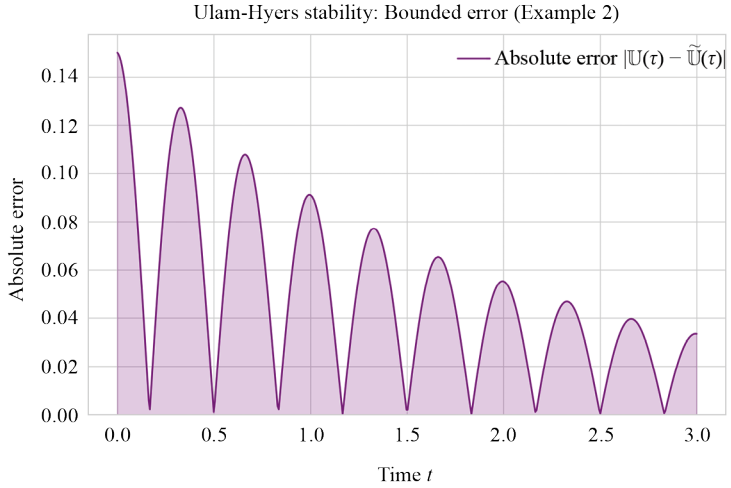

Figure 6. Absolute error for Example 2, confirming the Ulam-Hyers stability for a different model configuration

Table 2 presents the numerical values for the solution and error for Example 2.

Table 2. Numerical comparison for Example 2, based on the corresponding figure

Time (τ)	Unique solution ($\mathbb{U}(\tau)$)	Perturbed solution ($\tilde{\mathbb{U}}(\tau)$)	Absolute error
0.00	0.0000	0.0000	0.0000
0.50	0.5350	0.4011	0.1339
1.00	0.4817	0.5825	0.1008
1.50	0.5822	0.6130	0.0308
2.00	0.5214	0.5000	0.0214
2.50	0.3711	0.3805	0.0094
3.00	0.2833	0.2550	0.0283

5. An application: modeling a multi-stage epidemic

The utility of fractional operators in epidemiology is well-established, with recent applications including the modeling of lumpy skin disease using a Caputo-Fabrizio fractional SEIR framework [43]. The piecewise hybrid operator created in this paper has a complex structure that makes it a perfect tool for simulating intricate, real-world phenomena that change over time. One of the most relevant uses is in mathematical epidemiology, where government initiatives, behavioural shifts, and public awareness frequently modify the dynamics of an infectious illness. In order to represent the multi-stage evolution of an epidemic, we present a SEIR model that is guided by our piecewise operator.

5.1 *The piecewise SEIR model formulation*

Let the total population be $N(\tau) = S(\tau)+E(\tau)+I(\tau)+R(\tau)$. The state of the model at any time τ is described by the vector $\mathbb{U}(\tau) = [S(\tau), E(\tau), I(\tau), R(\tau)]^T$. The piecewise SEIR model is formulated as the following model of nonlinear differential equations:

$$\begin{cases} {}^{\mathscr{P}}\mathscr{D}^{\rho,\delta}_{[\tau]} S(\tau) = \Lambda - \dfrac{\delta_{inf} S(\tau) I(\tau)}{N(\tau)} - \mu S(\tau), \\ {}^{\mathscr{P}}\mathscr{D}^{\rho,\delta}_{[\tau]} E(\tau) = \dfrac{\delta_{inf} S(\tau) I(\tau)}{N(\tau)} - (\varepsilon+\mu) E(\tau), \\ {}^{\mathscr{P}}\mathscr{D}^{\rho,\delta}_{[\tau]} I(\tau) = \varepsilon E(\tau) - (\gamma+\mu+d) I(\tau), \\ {}^{\mathscr{P}}\mathscr{D}^{\rho,\delta}_{[\tau]} R(\tau) = \gamma I(\tau) - \mu R(\tau), \end{cases} \tag{14}$$

subject to non-negative initial conditions $S(a) \geq 0, E(a) \geq 0, I(a) > 0, R(a) \geq 0$. The parameters are defined as:

Λ: The recruitment rate into the susceptible population (e.g., births).

δ_{inf}: The disease transmission rate.

μ: The natural death rate.

ε: The rate at which exposed individuals become infectious (inverse of the mean incubation period).

γ: The recovery rate of infected individuals.

d: The disease-induced death rate.

The purpose of the proposed SEIR model is to mimic the dynamics of an acute infectious disease with a long incubation time that spreads throughout a community. For respiratory viruses, like influenza strains or new coronaviruses

(like Severe Acute Respiratory Syndrome Coronavirus 2 (SARS-CoV-2)), where a person can get infected and exposed (the E compartment) before becoming contagious (the I compartment), this structure works very well. The model's main strength is its ability to depict the course of an epidemic that triggers a robust and dynamic social reaction, rather than simulating a particular disease. Therefore, it is a perfect tool for examining how large policy changes, such as vaccination campaigns, and non-pharmaceutical interventions affect the spread of this disease.

The numerical simulation's parameter values are chosen based on biological plausibility and established in the literature on epidemiological modelling, rather than being suited to a particular historical outbreak. This strategy is used to guarantee that the simulation offers a qualitatively accurate and instructive illustration of the behaviour of the model. For example, the recovery rate, $\gamma = 1/14$, corresponds to a mean infectious time of 14 days, but the infectious rate, $\varepsilon = 1/7$, corresponds to a mean incubation period of 7 days. Standard population models serve as the basis for demographic parameters such as the natural death rate (μ) and recruitment rate (Λ). The most sensitive parameter is the transmission rate, δ_{inf}, which is selected to create a large initial outbreak that is subsequently managed in the following stages by the fractional operators' effects. This approach guarantees that the emphasis stays on showcasing the piecewise fractional framework's dynamic capabilities.

5.2 *Interpretation of the piecewise dynamics*

The primary strength of this model is its ability to map the mathematical structure of the operator to the real-world phases of an epidemic. We define the time interval $J = [a, T]$ with partitions at τ_1 and τ_2.

Phase 1: The Initial Outbreak ($\tau \in J_1 = [a, \tau_1]$).

Operator: Classical integer-order derivative.

Justification: The majority of the people is not aware of the new disease at the start of an outbreak. Neither government actions nor behavioural improvements are occurring. The classical derivative accurately describes the memoryless process by which the infection spreads. Similar to chemistry's rule of mass action, the rate of new infections is solely determined by the number of susceptible and contagious people present.

Phase 2: The Awareness and Behavioral Response Phase ($\tau \in J_2 = (\tau_1, \tau_2]$).

Operator: Atangana-Baleanu Caputo (ABC) derivative.

Justification: The public learns of the epidemic after time τ_1. Social distancing and mask-wearing are examples of spontaneous behavioural changes brought on by fear of infection, media coverage, and the memory of a recent increase in cases and deaths. Additionally, governments may enact initial, minimally invasive policies. The ABC derivative is ideal for capturing this memory effect because of its non-local and non-singular Mittag-Leffler kernel. The history of the epidemic during the period $[\tau_1, \tau]$ has an impact on the rate of transmission at time τ, which is no longer exclusively reliant on the state at time τ. The strength of this collective memory can be measured by the fractional order ρ.

Phase 3: The Major Intervention Phase ($\tau \in J_3 = (\tau_2, T]$).

Operator: Modified Atangana-Baleanu Caputo (MABC) derivative.

Justification: A major "game-changing" event that changes the model's memory's nature takes place at time τ_2. This may be a rigorous, enforced lockdown, the introduction of a new variety, or a widespread vaccination campaign. This fundamental change in the dynamics of the model is reflected in the transition to the MABC derivative, which has a different integral structure. This new phase is reflected in the new fractional order δ. A successful immunisation campaign, for example, may result in dynamics that are less reliant on long-range memory, bringing δ closer to 1.

5.3 *Connection to theoretical results*

A set of nonlinear differential equations is known as the SEIR model (14). The functions on the right-hand side are continuous and meet the Lipschitz requirements (H1) and (H2) under biologically realistic assumptions (e.g., bounded population). As a result, the theoretical foundation established in Section 3 is immediately applicable. Theorem 2 and Theorem 3, our key findings, ensure that this piecewise epidemiological model is well-posed, which means it has a unique solution that is stable against minor perturbations. This mathematical robustness is essential for the model to be a reliable tool for forecasting and policy evaluation.

6. Numerical analysis and simulation

We design a numerical technique to estimate the solution in order to show the behaviour of the suggested piecewise SEIR model (14) and demonstrate its usefulness.

6.1 *The numerical scheme*

The piecewise model (14) is solved numerically using a technique that can manage the change between several differential operator types. A piecewise predictor-corrector scheme based on the Adams-Bashforth-Moulton methodology is a reliable and popular method for these kinds of issues, and we modify it for every interval.

Let the time interval $J=[a,\,T]$ be discretized into M steps of size $h=\dfrac{T-a}{M}$, such that $\tau_n=a+nh$ for $n=0,\,1,\,\ldots,\,M$. Let $\mathbb{U}_n\approx\mathbb{U}(\tau_n)$ be the numerical approximation of the solution vector $\mathbb{U}(\tau)=[S(\tau),\,E(\tau),\,I(\tau),\,R(\tau)]^T$, and let $\mathscr{F}_n=\mathscr{F}(\tau_n,\,\mathbb{U}_n)$ denote the evaluation of the right-hand side of the model at step n.

Step 1: Classical Interval ($\tau_n\in J_1=[a,\,\tau_1]$). For the initial phase where the governing equation is ${}^{\mathscr{P}}\mathscr{D}_a^{\rho,\,\delta}\mathbb{U}(\tau)=\dfrac{d}{d\tau}\mathbb{U}(\tau)=\mathscr{F}(\tau,\,\mathbb{U}(\tau))$, we can use any standard Ordinary Differential Equations (ODE) solver. For simplicity and clarity, we present the forward Euler method, which is a first-order Adams-Bashforth scheme:

$$\mathbb{U}_{n+1}=\mathbb{U}_n+h\mathscr{F}(\tau_n,\,\mathbb{U}_n)\,. \tag{15}$$

This iterative process is applied for $n=0,\,1,\,\ldots,\,N_1-1$, where $\tau_{N_1}=\tau_1$, to obtain the solution $\mathbb{U}(\tau_1)\approx\mathbb{U}_{N_1}$.

Step 2: ABC Interval ($\tau_n\in J_2=(\tau_1,\,\tau_2]$). On this interval, the model is equivalent to the Volterra integral equation:

$$\mathbb{U}(\tau)=\mathbb{U}(\tau_1)+\frac{1-\rho}{B(\rho)}\mathscr{F}(\tau,\,\mathbb{U}(\tau))+\frac{\rho}{B(\rho)\Gamma(\rho)}\int_{\tau_1}^{\tau}(\tau-\upsilon)^{\rho-1}\mathscr{F}(\upsilon,\,\mathbb{U}(\upsilon))\,d\upsilon. \tag{16}$$

We solve this for $n=N_1,\,N_1+1,\,\ldots,\,N_2-1$, where $\tau_{N_2}=\tau_2$. To derive the predictor-corrector scheme, we evaluate (16) at $\tau=\tau_{n+1}$:

$$\mathbb{U}(\tau_{n+1})=\mathbb{U}(\tau_1)+\frac{1-\rho}{B(\rho)}\mathscr{F}(\tau_{n+1},\,\mathbb{U}(\tau_{n+1}))+\frac{\rho}{B(\rho)\Gamma(\rho)}\sum_{j=N_1}^{n}\int_{\tau_j}^{\tau_{j+1}}(\tau_{n+1}-\upsilon)^{\rho-1}\mathscr{F}(\upsilon,\,\mathbb{U}(\upsilon))\,d\upsilon.$$

The integral over $\left[\tau_j,\,\tau_{j+1}\right]$ is approximated using polynomial interpolation.

Now, we approximate the function $\mathscr{F}(\upsilon,\,\mathbb{U}(\upsilon))$ on the interval $\left[\tau_j,\,\tau_{j+1}\right]$ by a zero-order polynomial (a constant), $\mathscr{F}(\tau_j,\,\mathbb{U}_j)$. This leads to an explicit scheme.

$$\begin{aligned}\mathbb{U}_{n+1}^{P}&=\mathbb{U}_{N_1}+\frac{1-\rho}{B(\rho)}\mathscr{F}_n+\frac{\rho}{B(\rho)\Gamma(\rho)}\sum_{j=N_1}^{n}\mathscr{F}_j\int_{\tau_j}^{\tau_{j+1}}(\tau_{n+1}-\upsilon)^{\rho-1}\,d\upsilon\\&=\mathbb{U}_{N_1}+\frac{1-\rho}{B(\rho)}\mathscr{F}_n+\frac{\rho}{B(\rho)\Gamma(\rho+1)}\sum_{j=N_1}^{n}\mathscr{F}_j\left[(\tau_{n+1}-\tau_j)^{\rho}-\left(\tau_{n+1}-\tau_{j+1}\right)^{\rho}\right]\\&=\mathbb{U}_{N_1}+\frac{1-\rho}{B(\rho)}\mathscr{F}_n+\frac{\rho h^{\rho}}{B(\rho)\Gamma(\rho+1)}\sum_{j=N_1}^{n}\mathscr{F}_j\left[(n-j+1)^{\rho}-(n-j)^{\rho}\right].\end{aligned}$$

This predicted value $\mathbb{U}_{n+1}^{P}$ is then used to evaluate $\mathscr{F}_{n+1}^{P} = \mathscr{F}\left(\tau_{n+1}, \mathbb{U}_{n+1}^{P}\right)$.

To improve accuracy, we now approximate the integrand $\mathscr{F}(\upsilon, \mathbb{U}(\upsilon))$ over $\left[\tau_j, \tau_{j+1}\right]$ using a first-order polynomial (a line segment) connecting $(\tau_j, \mathscr{F}_j)$ and $\left(\tau_{j+1}, \mathscr{F}_{j+1}\right)$. This yields an implicit one-step scheme. The main correction comes from the last interval $[\tau_n, \tau_{n+1}]$, where we use the predicted value $\mathscr{F}_{n+1}^{P}$. The corrected value $\mathbb{U}_{n+1}$ is:

$$\mathbb{U}_{n+1} = \mathbb{U}_{N_1} + \frac{1-\rho}{B(\rho)}\mathscr{F}_{n+1}^{P}$$

$$+ \frac{\rho h^{\rho}}{B(\rho)\Gamma(\rho+2)} \sum_{j=N_1}^{n} \left(\mathscr{F}_j a_{j,n}^{\rho} + \mathscr{F}_{j-1} b_{j,n}^{\rho}\right)$$

$$+ \frac{\rho h^{\rho}}{B(\rho)\Gamma(\rho+2)} \left(\mathscr{F}_{n+1}^{P}(\rho) + \ldots\right),$$

where the coefficients $a_{j,n}^{\rho}$ and $b_{j,n}^{\rho}$ are derived from the interpolation. A simpler and common corrector form is:

$$\mathbb{U}_{n+1} = \mathbb{U}_{N_1} + \frac{1-\rho}{B(\rho)}\mathscr{F}_{n+1}^{P} + \frac{\rho h^{\rho}}{B(\rho)\Gamma(\rho+1)} \sum_{j=N_1}^{n-1} \left[(n-j+1)^{\rho} - (n-j)^{\rho}\right] \mathscr{F}_j$$

$$+ \frac{\rho h^{\rho}}{B(\rho)\Gamma(\rho+2)} \left((n-N_1+1)^{\rho}(\rho) - \ldots\right) \left(\frac{\mathscr{F}_{n+1}^{P} + \mathscr{F}_n}{2}\right).$$

For simplicity, we can use the predicted value $\mathbb{U}_{n+1}^{P}$ as the final approximation for the step. The process is repeated until we reach $\mathbb{U}_{N_2}$.

Step 3: MABC Interval ($\tau_n \in J_3 = (\tau_2, T]$). On the final interval, the governing integral equation is:

$$\mathbb{U}(\tau) = \mathbb{U}(\tau_2) + \frac{1-\delta}{B(\delta)}[\mathscr{F}(\tau, \mathbb{U}(\tau)) - \mathscr{F}(\tau_2, \mathbb{U}(\tau_2))]$$

$$+ \frac{\delta}{B(\delta)\Gamma(\delta)} \int_{\tau_2}^{\tau} (\tau-\upsilon)^{\delta-1} [\mathscr{F}(\upsilon, \mathbb{U}(\upsilon)) - \mathscr{F}(\tau_2, \mathbb{U}(\tau_2))] d\upsilon. \tag{17}$$

Let $\mathscr{G}(\tau, \mathbb{U}(\tau)) = \mathscr{F}(\tau, \mathbb{U}(\tau)) - \mathscr{F}(\tau_2, \mathbb{U}_{N_2})$. Evaluating at $\tau = \tau_{n+1}$ gives:

$$\mathbb{U}(\tau_{n+1}) = \mathbb{U}_{N_2} + \frac{1-\delta}{B(\delta)}\mathscr{G}(\tau_{n+1}, \mathbb{U}(\tau_{n+1})) + \frac{\delta}{B(\delta)\Gamma(\delta)} \sum_{j=N_2}^{n} \int_{\tau_j}^{\tau_{j+1}} (\tau_{n+1}-\upsilon)^{\delta-1} \mathscr{G}(\upsilon, \mathbb{U}(\upsilon)) d\upsilon.$$

The structure is identical to the ABC case, but with the function $\mathscr{G}$ instead of $\mathscr{F}$ and the initial point τ_2 instead of τ_1. Now, we approximate $\mathscr{G}(\upsilon, \mathbb{U}(\upsilon))$ on $[\tau_j, \tau_{j+1}]$ by the constant $\mathscr{G}_j = \mathscr{G}(\tau_j, \mathbb{U}_j)$.

$$\mathbb{U}_{n+1}^{P} = \mathbb{U}_{N_2} + \frac{1-\delta}{B(\delta)}\mathcal{G}_n + \frac{\delta h^{\delta}}{B(\delta)\Gamma(\delta+1)} \sum_{j=N_2}^{n} \mathcal{G}_j \left[(n-j+1)^{\delta} - (n-j)^{\delta}\right].$$

This gives the predicted value $\mathbb{U}_{n+1}^{P}$. Using the predicted value $\mathbb{U}_{n+1}^{P}$ to find $\mathcal{G}_{n+1}^{P} = \mathcal{G}\left(\tau_{n+1}, \mathbb{U}_{n+1}^{P}\right)$, we can form a more accurate implicit scheme. The Adams-Moulton formula adapted for this equation is:

$$\mathbb{U}_{n+1} = \mathbb{U}_{N_2} + \frac{1-\delta}{B(\delta)}\mathcal{G}_{n+1}^{P} + \frac{\delta h^{\delta}}{B(\delta)\Gamma(\delta+2)} \left(\mathcal{G}_{n+1}^{P} + \sum_{j=N_2}^{n} \left(\mathcal{G}_j a_{j,n}^{\delta} + \mathcal{G}_{j-1} b_{j,n}^{\delta}\right)\right),$$

where $a_{j,n}^{\delta}$ and $b_{j,n}^{\delta}$ are the Adams-Moulton coefficients. This scheme is iterated for $n = N_2, \ldots, M-1$ to obtain the complete solution over the interval J.

6.2 *Simulation results*

To visualize the solution, we simulate the model over a period of 150 days. The time interval is partitioned at $\tau_1 = 30$ days and $\tau_2 = 90$ days.

• Phase 1 ($0 \leq \tau \leq 30$): Classical derivative. An uncontrolled outbreak begins.

• Phase 2 ($30 < \tau \leq 90$): ABC derivative ($\rho = 0.9$). Represents a period of public awareness and moderate interventions (e.g., social distancing), leading to a slowdown in transmission. The memory effect captures the sustained behavioral change.

• Phase 3 ($90 < \tau < 150$): MABC derivative ($\delta = 0.98$). Represents a major intervention like a successful vaccination rollout, causing a fundamental shift in dynamics, pushing the model behavior closer to classical decay as the disease is brought under control.

We use the following biologically plausible parameters: $\Lambda = 20$, $\mu = 0.01$, $\delta_{inf} = 0.5$, $\varepsilon = 1/7$, $\gamma = 1/14$, and $d = 0.02$. The initial population is $N(0) = 100{,}000$, with $I(0) = 50$, $E(0) = 100$, $R(0) = 0$, and $S(0) = N(0) - E(0) - I(0) - R(0)$.

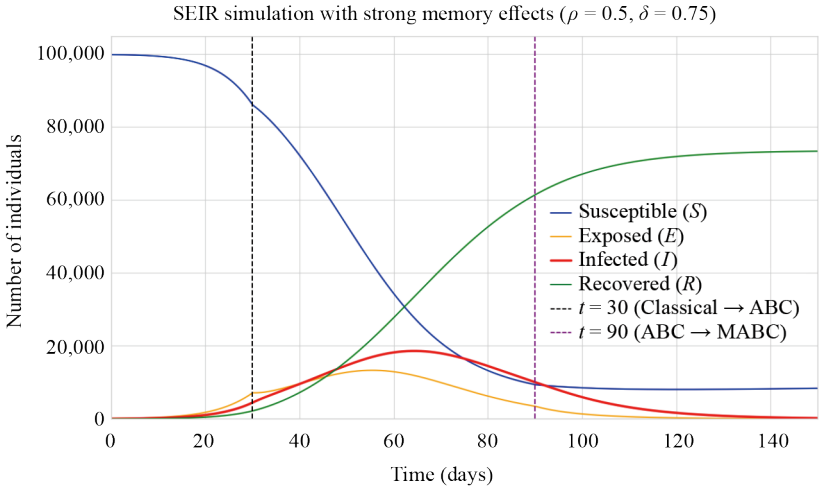

Figure 7. Numerical simulation of the piecewise SEIR model. The vertical dashed lines at $t = 30$ and $t = 90$ mark the transitions between the classical, ABC, and MABC dynamic phases

In Figure 7, the four compartments' dynamics are displayed. The number of infected people ($I(\tau)$, red curve) increases exponentially during Phase 1. The curve flattens at $\tau = 30$ as a result of switching to the ABC operator, illustrating the impact of interventions and societal memory. Although the infection peaks during this phase, it is far lower than it would have been in the absence of treatment. The switch to the MABC operator triggers a sharper drop in infected instances at $\tau = 90$, simulating the potent impact of a significant intervention such as vaccination. The model accurately depicts the multi-stage behaviour that characterises epidemics in the actual world.

6.3 *Sensitivity analysis with respect to fractional order*

One crucial parameter that measures the strength of the model's memory is the fractional order ρ in the ABC phase ($\tau \in J_2$). In an epidemiological context, a higher memory impact is indicated by a lower value of ρ, which can be read as a more effective and persistent public response to the epidemic. When $\rho = 1$, the traditional, memoryless situation is represented.

We simulate the SEIR model (14) for varying values of ρ throughout the intervention phase ($30 < \tau \leq 90$ days) in order to conduct a sensitivity analysis and examine the effect of this parameter. To compare these fractional possibilities to the traditional integer-order example ($\rho = 1.0$), we choose $\rho \in \{0.7, 0.8, 0.9\}$. Every other model parameter is unchanged from the last simulation.

The results are presented in Figure 8. Each subplot shows the evolution of one compartment (S, E, I, or R) for the different values of ρ.

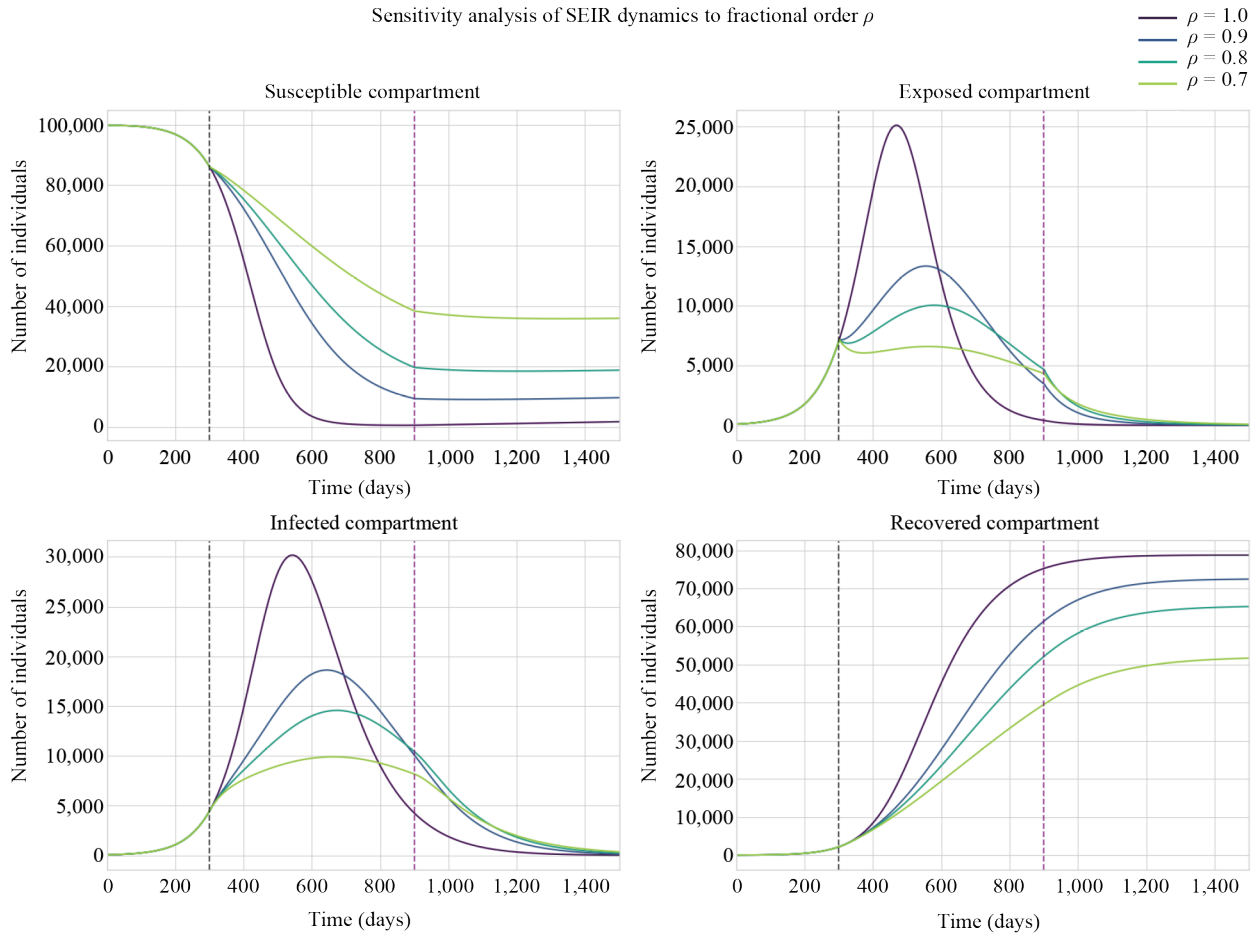

Figure 8. Dynamics of the Susceptible (S), Exposed (E), Infected (I), and Recovered (R) compartments for different fractional orders ρ during the intervention phase ($t \in (30, 90]$). The case $\rho = 1.0$ represents the classical derivative

The Infected (I) compartment plot provides the most important insights. It makes it very evident that a lower fractional order "flattens the curve". In comparison to the traditional example ($\rho = 1.0$), the infection peak is both delayed and significantly smaller for $\rho = 0.7$ (strongest memory). This closely relates to the public health objective of reducing the rate of transmission in order to avoid overburdening healthcare systems. The other compartments exhibit a similar pattern: the Recovered (R) population grows more gradually and the Susceptible (S) pool depletes more slowly for smaller ρ. This study demonstrates that the fractional order ρ is a useful and accessible metric for simulating the impact of long-term public health initiatives on societal memory.

We now examine the combined influence of the fractional orders in both the ABC and MABC phases to give a more thorough grasp of the dynamics of the model. We compare the model to the traditional integer-order case ($\rho = 1.0, \delta = 1.0$) by simulating the model for multiple pairs of (ρ, δ), where $\rho \in (0, 0.5]$ and $\delta \in (0.5, 0.9]$. This analysis shows how the trajectory of the epidemic is shaped by the interaction of the memory effects in the second and third phases.

The selected pairs represent a progression from weaker to stronger memory effects across both intervention periods.

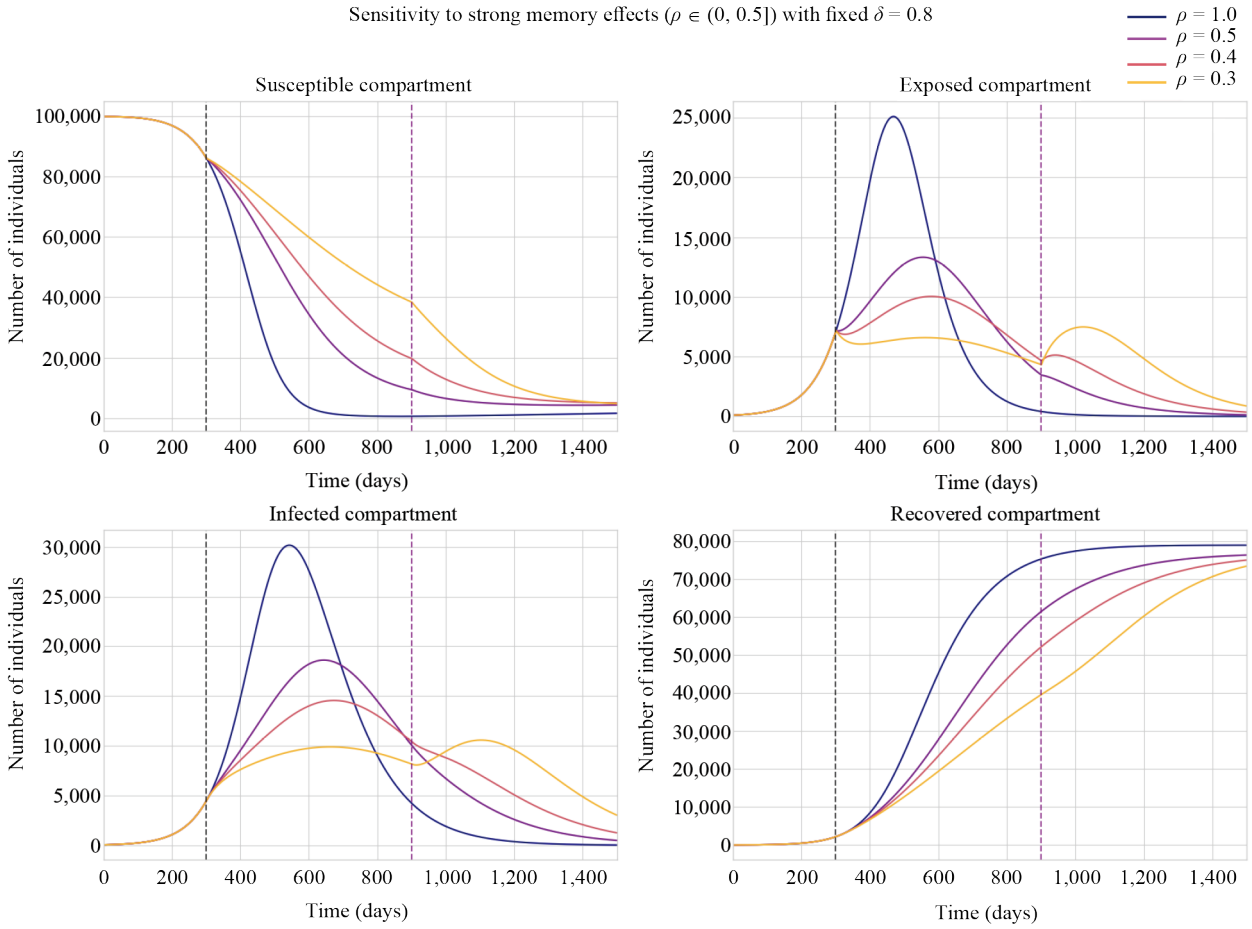

Figure 9. Combined sensitivity analysis showing the dynamics of each compartment for different pairs of fractional orders (ρ, δ)

Figure 9 shows the simulation results. The Infected (I) compartment's plot is very instructive. The epidemic curve gradually becomes suppressed as ρ and δ both drop. A lower ρ flattens the first peak in Phase 2, and a lower δ makes the ensuing decline in Phase 3 sharper and more definitive. The situation where $(\rho, \delta) = (0.3, 0.7)$ produces the greatest decrease in the overall number of infections, indicating a very successful, long-lasting public health response during

two different intervention phases. The model's ability to represent complex, multi-stage control techniques and their cumulative effect on disease dynamics is highlighted by this combined analysis.

7. Conclusions and future works

We have carried out a thorough qualitative examination of a new class of nonlinear FDEs in this paper. A complex model with a nested p-Laplacian operator and a multi-stage, piecewise hybrid fractional derivative governing it served as the central component of this study. With a sequential transition from the traditional integer-order derivative to the ABC derivative and then to the MABC derivative, this special operator was created to simulate models with dynamic regime transitions. Determining this complex model's theoretical well-posedness has been our main goal. This study's primary contributions were accomplished with success. Using the Banach Fixed-Point Theorem, we rigorously established requirements for the existence and uniqueness of the solution by reformulating the problem into an equivalent model of Volterra integral equations. Additionally, we proved that the model is stable in the U-H sense, which is a crucial finding that ensures the solution's resilience to minor perturbations. Numerical examples that corroborated the findings and demonstrated the behaviour of the solution were provided to support the theoretical results. An application to a multi-stage SEIR epidemic model showed how useful this framework is in practice. We demonstrated how an epidemic's discrete stages: an initial uncontrolled outbreak (classical phase), a period of public awareness and moderate intervention (ABC phase with memory effects), and a final stage of decisive control, like a vaccination campaign (MABC phase) can be successfully captured by the piecewise operator. The results of the sensitivity analysis also showed that the fractional orders ρ and δ are useful and intuitive metrics for measuring the efficacy and long-term effects of public health initiatives. This study brings up a number of interesting directions for further research. Potential directions include:

• Creation of High-Order Numerical Systems: Although a numerical approach was described, it would be beneficial to build and thoroughly analyse the convergence of a high-order predictor-corrector scheme for this particular piecewise model.

• Parameter Estimation and Real-World Data Fitting: An important next step to confirm this model's useful forecasting abilities would be to apply it to real-world data from an epidemic (such a particular wave of COVID-19) in order to estimate the fractional orders and other parameters.

• Extension to stochastic models: A more accurate depiction of the inherent randomness in disease transmission and other complex processes would be possible if stochastic effects were included in the model.

• Application to Other Fields: The theoretical framework developed here is general and could be used to model other multi-stage problems in engineering (analysing material fatigue under changing loads), environmental science [44], and finance (modelling market behaviour before and after a crisis).

In conclusion, this study offers a flexible and reliable mathematical tool for upcoming research into nonlinear models with dynamic and piecewise behaviour in addition to resolving a challenging theoretical issue.

Data availability

All data generated or analyzed during this study are included within this published article.

Acknowledgement

This study is supported via funding from Prince sattam bin Abdulaziz University project number (PSAU/2025/R/1447). The researchers wish to extend their sincere gratitude to the Deanship of Scientific Research at the Islamic University of Madinah.

Conflict of interest

The authors declare no competing financial interest.

References

[1] Podlubny I. *Fractional Differential Equations*. San Diego, CA, USA: Academic Press; 1999.

[2] Samko SG, Kilbas AA, Marichev OI. *Fractional Integrals and Derivatives*. Yverdon, Switzerland: Gordon & Breach; 1993.

[3] Magin RL. *Fractional Calculus in Bioengineering*. Redding, CA, USA: Begell House; 2006.

[4] Kilbas AA, Srivastava HM, Trujillo JJ. Theory and applications of fractional differential equations. In: *North-Holland Mathematics Studies*. Amsterdam, The Netherlands: Elsevier; 2006.

[5] Baleanu D, Diethelm K, Scalas E, Trujillo JJ. Fractional calculus. In: *Series on Complexity, Nonlinearity and Chaos*. Vol. 3. Hackensack, NJ, USA: World Scientific Publishing Co. Pte. Ltd.; 2012.

[6] Srivastava HM, Saad KM. Some new models of the time-fractional gas dynamics equation. *Advances in Mathematical Models and Applications*. 2018; 3: 5-17.

[7] Yadav P, Jahan S, Shah K, Peter OJ, Abdeljawad T. Fractional-order modelling and analysis of diabetes mellitus: utilizing the Atangana-Baleanu Caputo (ABC) operator. *Alexandria Engineering Journal*. 2023; 81: 200-209. Available from: https://doi.org/10.1016/j.aej.2023.09.006.

[8] Lee S, Kim H, Jang B. A novel numerical method for solving nonlinear fractional-order differential equations and its applications. *Fractal and Fractional*. 2024; 8(1): 65. Available from: https://doi.org/10.3390/fractalfract8010065.

[9] Caputo M, Fabrizio M. A new definition of fractional derivative without singular kernel. *Progress in Fractional Differentiation and Applications*. 2015; 1(2): 73-85.

[10] Atangana A, Baleanu D. New fractional derivatives with nonlocal and non-singular kernel: theory and application to heat transfer model. *Thermal Science*. 2016; 20(2): 763-769. Available from: https://doi.org/10.2298/TSCI160111018A.

[11] Ramaswamy R, Mani G, Kumar D, Ege O. Mathematical model of the monkeypox virus disease via ABC fractional order derivative. *CMES-Computer Modeling in Engineering and Sciences*. 2025; 143(2): 1843-1894. Available from: https://doi.org/10.32604/cmes.2025.063672.

[12] Mani G, Gnanaprakasam AJ, Ramalingam S, Omer AS, Khan I. Mathematical model of the lumpy skin disease using Caputo fractional-order derivative via invariant point technique. *Scientific Reports*. 2025; 15(1): 9112. Available from: https://doi.org/10.1038/s41598-025-92884-y.

[13] Janardhanan G, Mani G, Santina D, Mlaiki N. Existence and uniqueness theorems for nonlinear coupled boundary value problem of the ABC fractional differential equation. *Journal of Mathematics and Computer Science*. 2025; 37(3): 297-318. Available from: https://dx.doi.org/10.22436/jmcs.037.03.04.

[14] Mani G, Lakshmanan V, Mohideen ARK, Emadifar H. Existence and uniqueness results for the coupled pantograph system with Caputo fractional operator and Hadamard integral. *International Journal of Differential Equations*. 2025; 2025(1): 1202608. Available from: https://doi.org/10.1155/ijde/1202608.

[15] Aldwoah KA, Almalahi MA, Shah K. Theoretical and numerical simulations on the hepatitis B virus model through a piecewise fractional order. *Fractal and Fractional*. 2023; 7(12): 844. Available from: https://doi.org/10.3390/fractalfract7120844.

[16] Khan H, Alzabut J, Alfwzan WF, Gulzar H. Nonlinear dynamics of a piecewise modified ABC fractional-order leukemia model with symmetric numerical simulations. *Symmetry*. 2023; 15(7): 1338. Available from: https://doi.org/10.3390/sym15071338.

[17] Atangana A, Araz Sİ. New concept in calculus: piecewise differential and integral operators. *Chaos, Solitons & Fractals*. 2021; 145: 110638. Available from: https://doi.org/10.1016/j.chaos.2020.110638.

[18] Madani YA, Almalahi MA, Osman O, Muflh B, Aldwoah K, Mohamed KS, et al. Analysis of an acute diarrhea piecewise modified ABC fractional model: optimal control, stability and simulation. *Fractal and Fractional*. 2025; 9(2): 68. Available from: https://doi.org/10.3390/fractalfract9020068.

[19] Clemente-Lopez D, Munoz-Pacheco JM, Zambrano-Serrano E, Félix Beltrán OG, Rangel-Magdaleno JDJ. A piecewise linear approach for implementing fractional-order multi-scroll chaotic systems on ARMs and FPGAs. *Fractal and Fractional*. 2024; 8(7): 389. Available from: https://doi.org/10.3390/fractalfract8070389.

[20] Aly ES, Almalahi MA, Aldwoah KA, Shah K. Criteria of existence and stability of an *n*-coupled system of generalized Sturm-Liouville equations with a modified ABC fractional derivative and an application to the SEIR influenza epidemic model. *AIMS Mathematics*. 2024; 9(6): 14228-14252. Available from: https://doi.org/10.3934/math.2024691.

[21] Aldwoah KA, Almalahi MA, Shah K, Awadalla M, Egami RH. Dynamics analysis of dengue fever model with harmonic mean type under fractal-fractional derivative. *AIMS Mathematics*. 2024; 9(6): 13894-13926. Available from: https://doi.org/10.3934/math.2024676.

[22] Alraqad T, Almalahi MA, Mohammed N, Alahmade A, Aldwoah KA, Saber H. Modeling Ebola dynamics with a Φ-piecewise hybrid fractional derivative approach. *Fractal and Fractional*. 2024; 8(10): 596. Available from: https://doi.org/10.3390/fractalfract8100596.

[23] Vázquez JL. *The Porous Medium Equation: Mathematical Theory*. Oxford, UK: Clarendon Press; 2006.

[24] Barles G. Nonlinear diffusion equations and applications. In: *An Introduction to the Theory of Viscosity Solutions for First-Order Hamilton-Jacobi Equations and Applications*. Heidelberg, Germany: Springer; 2008. p.1-75.

[25] Ayadi S, Ege O. Existence of solution for a Dirichlet boundary value problem involving the $p(x)$ Laplacian via a fixed point approach. *Miskolc Mathematical Notes*. 2022; 23(1): 85-92. Available from: https://doi.org/10.18514/MMN.2022.4101.

[26] Li C, Guo L. Positive solution pairs for coupled *p*-Laplacian Hadamard fractional differential model with singular source item on time variable. *Fractal and Fractional*. 2024; 8: 682. Available from: https://doi.org/10.3390/fractalfract8120682.

[27] Zhou J, Gong C, Wang W. The sign-changing solution for fractional (p, q)-Laplacian problems involving supercritical exponent. *Fractal and Fractional*. 2024; 8(4): 186. Available from: https://doi.org/10.3390/fractalfract8040186.

[28] Rahman SU, Díaz Palencia JL. Analytical and computational approaches for bi-stable reaction and *p*-Laplacian diffusion flame dynamics in porous media. *Mathematics*. 2024; 12(2): 216. Available from: https://doi.org/10.3390/math12020216.

[29] Yang D, Bai Z, Bai C. Existence of solutions for nonlinear Choquard equations with (p, q)-Laplacian on finite weighted lattice graphs. *Axioms*. 2024; 13(11): 762. Available from: https://doi.org/10.3390/axioms13110762.

[30] Hasanov M. Initial value problems for fractional *p*-Laplacian equations with singularity. *AIMS Mathematics*. 2024; 9(5): 12800-12813. Available from: https://doi.org/10.3934/math.2024625.

[31] Ahmadkhanlu A, Afshari H, Alzabut J. A new fixed point approach for solutions of a *p*-Laplacian fractional *q*-difference boundary value problem with an integral boundary condition. *AIMS Mathematics*. 2024; 9(9): 23770-23785. Available from: https://doi.org/10.3934/math.20241155.

[32] Li W, Wang G, Li G. The local boundary estimate of weak solutions to fractional *p*-Laplace equations. *AIMS Mathematics*. 2025; 10(4): 8002-8021. Available from: https://doi.org/10.3934/math.2025367.

[33] Kaushik K, Kumar A, Khan A, Abdeljawad T. Existence of solutions by fixed point theorem of general delay fractional differential equation with *p*-Laplacian operator. *AIMS Mathematics*. 2023; 8(5): 10160-10176. Available from: https://doi.org/10.3934/math.2023514.

[34] Boulaaras S, Guefaifia R, Cherif B, Radwan T. Existence result for a Kirchhoff elliptic system involving *p*-Laplacian operator with variable parameters and additive right hand side via sub and super solution methods. *AIMS Mathematics*. 2021; 6(3): 2315-2329. Available from: https://doi.org/10.3934/math.2021140.

[35] Yao W, Zhang H. Multiple solutions for *p*-Laplacian fractional differential equations with psi Caputo derivative and impulsive effects. *Journal of Applied Analysis & Computation*. 2025; 15(6): 3480-3503. Available from: https://doi.org/10.11948/20250024.

[36] Khan H, Alzabut J, Gulzar H, Tunç O, Pinelas S. On system of variable order nonlinear *p*-Laplacian fractional differential equations with biological application. *Mathematics*. 2023; 11(8): 1913. Available from: https://doi.org/10.3390/math11081913.

[37] Saber H, Almalahi MA, Albala H, Aldwoah K, Alsulami A, Shah K, et al. Investigating a nonlinear fractional evolution control model using W-piecewise hybrid derivatives: an application of a breast cancer model. *Fractal and Fractional*. 2024; 8(12): 735. Available from: https://doi.org/10.3390/fractalfract8120735.

[38] Refai O, Almalki SSE, Abualnaja KM. A modified Atangana-Baleanu fractional derivative with application. *Advances in Difference Equations*. 2020; 2020(1): 574.

[39] Al-Refai M, Baleanu D. On an extension of the operator with Mittag-Leffler kernel. *Fractals*. 2022; 30(05): 2240129. Available from: https://doi.org/10.1142/S0218348X22401296.

[40] Al-Refai M. Proper inverse operators of fractional derivatives with nonsingular kernels. *Reports of the Palermo Mathematical Circle Series 2*. 2022; 71(2): 525-535. Available from: https://doi.org/10.1007/s12215-021-00638-2.

[41] Rezapour S, Thabet STM, Matar MM, Alzabut J, Etemad S. Some existence and stability criteria to a generalized FBVP having fractional composite *p*-Laplacian operator. *Journal of Function Spaces*. 2021; 2021(1): 9554076. Available from: https://doi.org/10.1155/2021/9554076.

[42] Khan H, Tunc C, Chen W, Khan A. Existence theorems and Hyers-Ulam stability for a class of hybrid fractional differential equations with *p*-Laplacian operator. *Journal of Applied Analysis and Computation*. 2018; 8(4): 1211-1226. Available from: https://doi.org/10.11948/2018.1211.

[43] Ramaswamy R, Mani G, Mohanraj R, Ege O. Mathematical SEIR model of the lumpy skin disease using Caputo-Fabrizio fractional-order. *European Journal of Pure and Applied Mathematics*. 2025; 18(2): 5933. Available from: https://doi.org/10.29020/nybg.ejpam.v18i2.5933

[44] Ramaswamy R, Mani G, Palanisamy S, Ege O. Mathematical model of the waste plastic management via ABC fractional order derivative. *International Journal of Mathematics and Mathematical Sciences*. 2025; 2025(1): 9204263. Available from: https://doi.org/10.1155/ijmm/9204263.